Applied Physics Reviews

Toward "hereditary epidemiology": A temporal Boltzmann approach to COVID-19 fatality trends

Cite as: Appl. Phys. Rev. **8**, 041417 (2021); https://doi.org/10.1063/5.0062867
Submitted: 09 July 2021 • Accepted: 21 October 2021 • Published Online: 22 December 2021

Niketa Ukaj, Stefan Scheiner and Christian Hellmich

Applied Physics Reviews ARTICLE scitation.org/journal/are

Toward "hereditary epidemiology": A temporal Boltzmann approach to COVID-19 fatality trends

Cite as: Appl. Phys. Rev. 8, 041417 (2021); doi: 10.1063/5.0062867
Submitted: 9 July 2021 · Accepted: 21 October 2021 ·
Published Online: 22 December 2021

Niketa Ukaj, Stefan Scheiner, and Christian Hellmich[a)]

AFFILIATIONS

Institute for Mechanics of Materials and Structures, TU Wien, Vienna, Austria

[a)]Author to whom correspondence should be addressed: christian.hellmich@tuwien.ac.at

ABSTRACT

Countless research contributions reflect two major concepts for modeling the spread of the COVID-19 pandemic: (i) ordinary differential equations for population compartments, such as infected or deceased persons (these approaches often exhibit limited predictive capabilities); and (ii) rules applied to digitally realized agents in the populations (these approaches often lack reliable input data and may become computationally overly expensive). As a remedy, we here introduce and discuss convolutional integrodifferential equations adapted from Boltzmann's hereditary mechanics, so as to predict COVID-19 fatality trends from the evolutions of newly infected persons. Replacing the classical statistical reasoning by deliberations arising from the notion of "virus loads" and the corresponding compliance of the infected population to these loads, model errors with respect to data recorded in 102 countries, territories, or US states can be drastically reduced, namely, up to 98% when compared to the traditional kinetics equation of Kermack and McKendrick. The coefficients of determination between model predictions and recorded data range from 94% to 100%, a precision hitherto unachieved in equation-based epidemic modeling.

I. INTRODUCTION

With the advent of the COVID-19 pandemic, mathematical modeling of disease spreading has experienced an unprecedented boost, along with a lively debate on its potentials and limitations.[1] Broadly speaking, two classes of models have seen massive use in this context: (i) compartment models, also referred to as "susceptible–infected–removed (SIR)" models, based on ordinary differential equations[2–8] as originally proposed in the landmark paper of Kermack and McKendrick,[9] and (ii) agent-based models based on computationally implemented rules governing the interaction of very many entities.[10–12] The main argument put forward in favor of the second type of models is the limitation of ordinary differential equations when it comes to represent complex disease spreading events.[13] The classically employed ordinary differential equations express that the temporal derivative at a particular time instant, of each of the three population compartments (S, I, and R), solely depends on the size of the compartments S and I at the very same time instant. In order to overcome this limitation, roughly four types of improvements (and combinations thereof) have been proposed:

1. introducing additional compartments, including the exposed (E), the hospitalized (H), or the quarantined (Q);[14–18]
2. replacing the ordinary by partial differential equations where the compartments are resolved into spatially distributed population densities of persons undergoing different health and illness stages, and where the temporal derivatives of these population densities depend not only on their local magnitude, but also on the spatial gradients of the latter;[19]
3. replacing the classical ordinary by delay differential equations where the rate of one compartment size at a particular time instant depends on one or several compartment sizes at one or several earlier time instants;[20–24]
4. including statistical deliberations in terms of integrodifferential equations, where either the aforementioned single time instants are extended to a distribution of infinitely many such earlier time instants;[25,26] or where the compartments themselves are further resolved with respect to additional, statistically distributed attributes related to social heterogeneity in terms of contact or age.[27–29]

Typically, the aforementioned extensions of the SIR models aim at an improved representation of the person-to-person virus transmission dynamics for which statistical deliberations appear as very appropriate. Much less discussed are the limitations of the SIR models (and their extensions) when it comes to modeling the effect of the virus within the infected persons, that is, to more deeply exploring the relation between the infected and the removed. This is the focus of the present study, where we propose a fundamentally different approach to the problem: rather than resting on statistical deliberations having their origin in transmission dynamics, we resort to the very first physical problem which was tackled by means of integrodifferential equations: it was the famous Austrian physicist Ludwig Boltzmann,[30–32] who, as early as 1874, introduced integrodifferential equations in the context of hereditary mechanics and the so-called "elastic aftereffect," based on pioneering experimental work in material mechanics.[33–42] These integrodifferential equations express that the response of a system does not only depend on its current state, but also on the entire "loading" history it underwent before.

In the realm of continuum mechanics, the key integrodifferential equation is often referred to as the "Boltzmann superposition principle," which mathematically reads as[43–46]

$$\boldsymbol{\varepsilon}(t) = \int_{-\infty}^{t} \mathbb{J}(t-\tau) : \dot{\boldsymbol{\sigma}}(\tau)\, \mathrm{d}\tau, \tag{1}$$

where τ denotes the time instant where the rates of the second-order stress tensor $\boldsymbol{\sigma}(\tau)$ have been applied to the investigated material, $\dot{(\cdot)}$ denotes the temporal derivatives of quantity $(\cdot)$, $\mathbb{J}(t-\tau)$ denotes the fourth-order creep function tensor describing the time-dependent behavior of the investigated material loaded at time τ, $\mathbb{J}(t-\tau) \equiv 0$ for $t < \tau$, the symbol ":" is the second-order tensor contraction operator, and t denotes the time when the second-order strain tensor $\boldsymbol{\varepsilon}$ is recorded. Equation (1) expresses that the mechanical strain a viscoelastic material is experiencing at a certain point in time does not only depend on the mechanical stress at this time, but also on the stress history it has experienced hitherto. Equation (1) is also applied in cases where temporal stress discontinuities ("load steps" or finite stress increments $\Delta\boldsymbol{\sigma}_i$) occur; at corresponding time point τ_i, we have

$$\dot{\boldsymbol{\sigma}}(\tau_i) = \delta(\tau - \tau_i) \times \Delta\boldsymbol{\sigma}_i, \tag{2}$$

with δ standing for the Dirac delta function, being zero everywhere except for the origin, where its value is infinite, with the integral over this infinity amounting to one. For N_i of such load steps, and any other temporal variations of the stresses being absent, insertion of Eq. (2) into Eq. (1) yields

$$\boldsymbol{\varepsilon}(t) = \sum_{i=1}^{N_i} \mathbb{J}(t-\tau_i) : \Delta\boldsymbol{\sigma}(\tau_i). \tag{3}$$

Equations (1) and (3) take a central position in the rheology of hard and soft solids, including cementitious materials,[47,48] polymers,[49] and various biological materials.[50,51] The focus of the present paper is to transfer Boltzmann's "hereditary concept" from continuum mechanics to epidemiology, thereby introducing the notion of hereditary epidemiology: accordingly, we replace the piece of material with a human population exposed to an epidemic, the stress rate with an infection rate $\dot{C}$ ("number of confirmed cases per day"), and the stress history with the fatality trend $F(t)$. This gives rise to a new epidemiologic quantity, the fatality function $J_{\mathrm{F}}(t-\tau)$: it quantifies the number of fatalities over time, within all the individuals who were infected at time τ. Mathematically, our proposition reads as

$$F_{\mathrm{HER}}(t) = \int_{-\infty}^{t} J_{\mathrm{F}}(t-\tau) \times \dot{C}(\tau)\, \mathrm{d}\tau, \tag{4}$$

where the subscript "HER" refers to "hereditary," in order to distinguish the new modeling approach from reference models to which we will compare its predictive capabilities. In this sense, the remainder of the present paper is organized as follows: first, the novel epidemiologic integrodifferential equations are outlined in Sec. II, together with the transition from the logistic to Heaviside fatality functions and with a traditional ordinary differential equation as a reference model. This is followed by a collection of data recorded during the COVID-19 pandemic, as a basis for the model validation strategy described in Sec. III. Corresponding results are documented in Sec. IV and discussed in Sec. V, which also concludes the paper.

II. EPIDEMIOLOGICAL INTEGRODIFFERENTIAL EQUATIONS: LOGISTIC FATALITY FRACTIONS, "DELAY LIMIT," AND KINETIC REFERENCE MODEL

For the definition of $J_{\mathrm{F}}(t-\tau)$, we recall that in many cases biological processes can be reasonably well described by means of so-called logistic functions.[52–54] In particular, in order to consider the growth of death-inducing viruses within that portion of the population, which has been infected at time instant τ, we adopt the following mathematical format for J_{F}:

$$J_{\mathrm{F}}(t-\tau) = \frac{f_{\mathrm{F,HER}}}{1 + \exp\left[-s_{\mathrm{HER}} \times (t - \tau - T_{\mathrm{F,HER}})\right]}, \tag{5}$$

where $f_{\mathrm{F,HER}}$ is the hereditary model-related fatality fraction, $T_{\mathrm{F,HER}}$ is the hereditary model-related characteristic time of fatal illness, and s_{HER} is the shape parameter of the logistic function. Inserting Eq. (5) into Eq. (4) yields

$$F_{\mathrm{HER}}(t) = \int_{-\infty}^{t} \frac{f_{\mathrm{F,HER}} \times \dot{C}(\tau)}{1 + \exp\left[-s_{\mathrm{HER}} \times (t - \tau - T_{\mathrm{F,HER}})\right]}\, \mathrm{d}\tau. \tag{6}$$

Notably, the model defined by Eq. (6) requires, as input data, the temporal derivatives of the total number C of infected persons (also referred to as "confirmed cases"). However, these rates are typically accessible in incremental format, as detailed in Sec. III. Hence, it makes sense to reformulate Eq. (6) in terms of Dirac-type derivatives as seen in Eq. (2). In more detail, let us consider one particular increment of the total number of confirmed cases, termed $\Delta C(\tau_i)$—the newly confirmed cases at time τ_i. Then, the corresponding fatality evolution follows for time instants $t \geq \tau_i$ as

$$F_{\mathrm{HER}}[t, \Delta C(\tau_i)] = \frac{f_{\mathrm{F,HER}} \times \Delta C(\tau_i)}{1 + \exp\left[-s_{\mathrm{HER}} \times (t - \tau_i - T_{\mathrm{F,HER}})\right]}, \tag{7}$$

whereas $F_{\mathrm{HER}}(t, \tau_i) = 0$ if $t < \tau_i$. The overall fatality trend is eventually obtained through summing up all fatality evolutions due to single increments $\Delta C(\tau_i)$. Thus,

$$F_{\mathrm{HER}}(t) = \sum_{i=1}^{N_i} F_{\mathrm{HER}}[t, \Delta C(\tau_i)], \tag{8}$$

with N_i now standing for the number of time instants at which new increments $\Delta C(\tau_i)$ were recorded. Figure 1 shows schematically how the model defined by Eqs. (7) and (8) yields the overall fatality trend based on three increments of confirmed cases; namely, $\Delta C(\tau_1)$, $\Delta C(\tau_2)$, and $\Delta C(\tau_3)$. The fatality fraction $f_{\mathrm{F,HER}}$ needs additional attention: it quantifies how many of the people infected at time τ_i will eventually die. Hence, it is strongly influenced by medical and healthcare progress made during the investigated pandemic; and the latter progress might influence the characteristic time of fatal illness and the shape parameter as well. In the present paper, we focus on COVID-19 data recorded until the end of the year 2020, where most of the countries documenting the spread of the disease have experienced two infection waves of quite distinct nature: in most of these countries, the first waves (observed in the first half of 2020) were intercepted by comparably strict measures, whereas the second waves (starting sometime in the third quarter of 2020) struck with much higher infection numbers. At the same time, the disease characteristics differed significantly between the first and second waves; on the one hand, due to the above-mentioned progress in medical treatment options, and, on the other hand, due to changed infection distributions among the populations. In order to take these effects into account, we divide the total time domain into two time intervals, the first time interval corresponding to the first wave, and the second time interval corresponding to the second wave. Within each time interval, the increments of confirmed cases translate into corresponding fatalities based on Eqs. (7) and (8). Hence, denoting the time instant at which the first wave ends and the second wave begins by t_{wtr} (with subscript "wtr" standing for wave transition), Eq. (7) needs to be extended as follows:

$$\text{for } \tau_i \le t_{\mathrm{wtr}}: \quad F^{\mathrm{I}}_{\mathrm{HER}}[t, \Delta C(\tau_i)] = \frac{f^{\mathrm{I}}_{\mathrm{F,HER}} \times \Delta C(\tau_i)}{1 + \exp\left[-s^{\mathrm{I}}_{\mathrm{HER}} \times (t - \tau_i - T^{\mathrm{I}}_{\mathrm{F,HER}})\right]}, \tag{9}$$

and

$$\text{for } \tau_i > t_{\mathrm{wtr}}: \quad F^{\mathrm{II}}_{\mathrm{HER}}[t, \Delta C(\tau_i)] = \frac{f^{\mathrm{II}}_{\mathrm{F,HER}} \times \Delta C(\tau_i)}{1 + \exp\left[-s^{\mathrm{II}}_{\mathrm{HER}} \times (t - \tau_i - T^{\mathrm{II}}_{\mathrm{F,HER}})\right]}, \tag{10}$$

with parameters $f^{\mathrm{I}}_{\mathrm{F,HER}}$, $s^{\mathrm{I}}_{\mathrm{HER}}$, $T^{\mathrm{I}}_{\mathrm{F,HER}}$, $f^{\mathrm{II}}_{\mathrm{F,HER}}$, $s^{\mathrm{II}}_{\mathrm{HER}}$, and $T^{\mathrm{II}}_{\mathrm{F,HER}}$ being independent of each other. The overall fatality trend eventually follows from summing up the fatality trends associated with increments of confirmed cases occurring both during the first and the second wave

$$F_{\mathrm{HER2}}(t) = \sum_{i=1}^{N^{\mathrm{I}}_i} F^{\mathrm{I}}_{\mathrm{HER}}[t, \Delta C(\tau_i)] + \sum_{i=N^{\mathrm{I}}_i+1}^{N_i} F^{\mathrm{II}}_{\mathrm{HER}}[t, \Delta C(\tau_i)], \tag{11}$$

with N^{I}_i referring to the number of time instants at which new case increments were recorded during the first wave. As concerns the definition of t_{wtr}, we consider the local minimum of the 30-day moving average of newly confirmed infections between the two infection peaks.

Next, we are interested in the limit case where all fatally infected people die at exactly the same time, actually after a time period T_{DEL} after the infection, with "DEL" standing for delay. This limit case is associated with the shape parameter s going to infinity, and considering $s \to \infty$ in Eq. (5) yields a fatality function of the format

$$J_{\mathrm{F,DEL}}(t - \tau) = f_{\mathrm{F,DEL}} \times H(t - \tau - T_{\mathrm{F,DEL}}), \tag{12}$$

whereby H stands for the Heaviside function, reading as

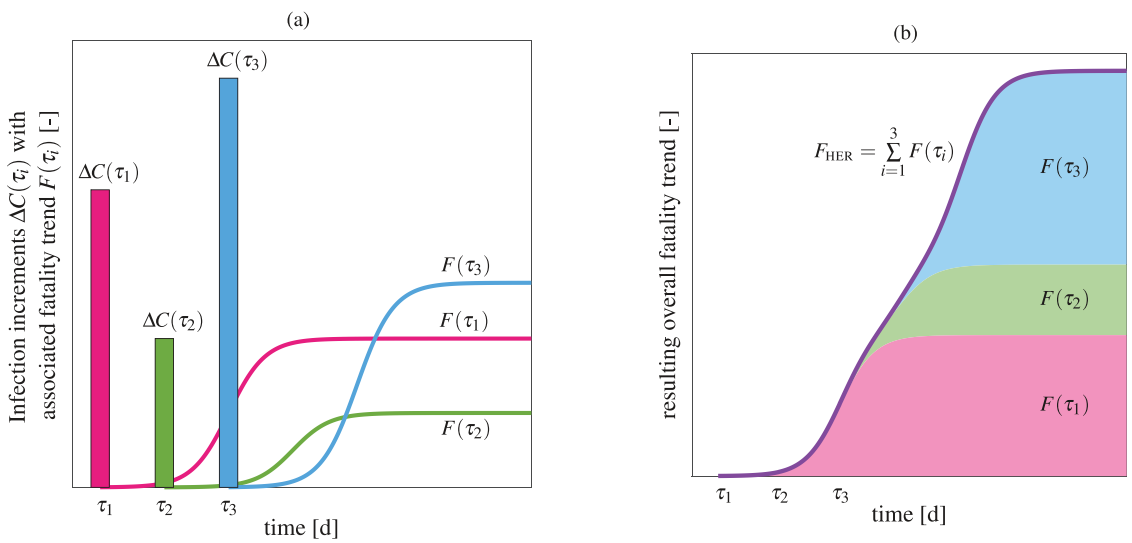

FIG. 1. Boltzmann superposition principle in the context of hereditary epidemiology: (a) examples for increments of confirmed cases, $\Delta C(\tau_1)$, $\Delta C(\tau_2)$, $\Delta C(\tau_3)$, and the corresponding contributions to the overall fatality trend, $F(\tau_1)$, $F(\tau_2)$, $F(\tau_3)$; the latter follow from Eq. (7), and are based on the same fatality fraction $f_{\mathrm{F,HER}}$, the same shape parameters s_{HER}, and the same characteristic times of fatal illness $T_{\mathrm{F,HER}}$; (b) the sum of the individual fatality trends results in the overall fatality trend $F_{\mathrm{HER}}(t)$, according to Eq. (8).

$$H(x) = \begin{cases} 0 & \text{for } x < 0, \\ \frac{1}{2} & \text{for } x = 0, \\ 1 & \text{for } x > 0. \end{cases} \tag{13}$$

Further simplification may be reached by omitting the convolution integral in Eq. (4) and replacing the confirmed case increments by the total number of confirmed cases, leading to the very simple expression

$$F_{\mathrm{DEL}}(t) = f_{\mathrm{F,DEL}} \times C(t - T_{\mathrm{F,DEL}}), \tag{14}$$

a format which we have recently described and discussed in greater detail;[55] thereby, $f_{\mathrm{F,DEL}}$ is the delay model-related fatality fraction, and $T_{\mathrm{F,DEL}}$ is the delay model-related characteristic time of fatal illness.

As a further model reference, we consider the equation standardly used in SIR models for relating the increase in fatalities at time instant t to the number of currently infected people at the very same time instant. Mathematically, this death kinetics law reads typically as follows:[9,56]

$$\frac{\mathrm{d}F_{\mathrm{KIN}}(t)}{\mathrm{d}t} = \beta_{\mathrm{F}} \times I(t), \tag{15}$$

where F_{KIN} is the kinetics model-predicted number of fatalities, I is the number of currently infected people, and $\beta_{\mathrm{F,KIN}}$ is the death rate parameter,[6] also referred to as mortality rate.[16] Alternatively, Eq. (15) can be formulated in incremental manner, yielding

$$\Delta F_{\mathrm{KIN}}(t_j) = F_{\mathrm{KIN}}(t_j) - F_{\mathrm{KIN}}(t_{j-1}) = \beta_{\mathrm{F}} \times I(t_{j-1}). \tag{16}$$

III. MODEL VALIDATION STRATEGY, BASED ON DATA COLLECTED DURING THE COVID-19 PANDEMIC

Ever since COVID-19 was declared a pandemic, the basic disease-characterizing data have been made available on various, publicly accessible platforms. For the mathematical model presented in Sec. II, the following data are particularly relevant: the total (cumulated) cases of people infected with COVID-19 until the respective dates, denoted by C; the active cases of (currently) infected people at the respective dates, denoted by I; the total (cumulated) deaths until the respective dates, denoted by F; the total (cumulated) recoveries until the respective date, denoted as R; and the corresponding daily changes ΔC, ΔI, ΔF, and ΔR. In this paper, we focus on countries where the reported numbers of fatalities are large enough to be statistically significant, yielding a sufficiently smooth time course of F. As related (quantitative) criterion, we have considered only countries with fatality numbers >80. As of December 31, 2020, this applies to the following 102 countries, territories, or US states (given in alphabetical order): Afghanistan, Albania, Andorra, Arizona, Arkansas, Armenia, Australia, Austria, Azerbaijan, Bahrain, Bangladesh, Belarus, Belgium, Bolivia, Bosnia and Herzegovina, Brazil, Bulgaria, California, Canada, Chile, China, Colorado, Connecticut, Costa Rica, Cote d'Ivoire, Croatia, Czechia, Delaware, Democratic Republic of the Congo, Denmark, Dominican Republic, Ecuador, Egypt, El Salvador, Estonia, Eswatini, Finland, France, Germany, Ghana, Greece, Haiti, Hawaii, Hungary, Indonesia, Ireland, Israel, Italy, Kansas, Kazakhstan, Kenya, Kosovo, Malawi, Malaysia, Massachusetts, Mauritania, Mexico, Michigan, Minnesota, Montenegro, Morocco, Namibia, Nebraska, Nepal, New Hampshire, New Jersey, New Mexico, New York, Nigeria, North Macedonia, Norway, Ohio, Oman, Panama, Pakistan, Paraguay, Pennsylvania, Peru, Poland, Portugal, Qatar, Rhode Island, Romania, Russia, Senegal, Somalia, South Africa, South Dakota, State of Palestine, Sudan, Suriname, Switzerland, Tennessee, Texas, Turkey, United Arab Emirates, Utah, Uzbekistan, Virginia, Wisconsin, Zambia, and Zimbabwe. The data related to Kosovo were collected from a Kosovo-specific website,[57] while the data related to all other countries or territories were collected from the reference website Worldometer[58] (which does not provide Kosovo-related data). For the purpose of reproducibility, all raw data used in this study are included in the supplementary material attached to this paper.

These data are employed for the determination of optimized model parameters, namely, $f_{\mathrm{F,HER}}^{\mathrm{opt}}$, $T_{\mathrm{F,HER}}^{\mathrm{opt}}$, and $s_{\mathrm{HER}}^{\mathrm{opt}}$ entering Eqs. (7) and (8), $f_{\mathrm{F,HER}}^{\mathrm{I,opt}}$, $T_{\mathrm{F,HER}}^{\mathrm{I,opt}}$, $s_{\mathrm{HER}}^{\mathrm{I,opt}}$, $f_{\mathrm{F,HER}}^{\mathrm{II,opt}}$, $T_{\mathrm{F,HER}}^{\mathrm{II,opt}}$, $s_{\mathrm{HER}}^{\mathrm{II,opt}}$ entering Eqs. (9)–(11), $f_{\mathrm{F,DEL}}^{\mathrm{opt}}$, $T_{\mathrm{F,DEL}}^{\mathrm{opt}}$ entering Eq. (14), and $\beta_{\mathrm{F}}^{\mathrm{opt}}$ entering Eq. (16). To that end, we considered the temporal average over the absolute errors between modeled and recorded fatalities. At time point t_i, the aforementioned absolute errors read as

$$\mathscr{E}_{m,i} = |F_m(t_i) - F(t_i)|, \tag{17}$$

if $m = \mathrm{HER}, \mathrm{DEL}, \mathrm{HER2}, \mathrm{DEL2}$, with $F_m(t_i)$ and $F(t_i)$ standing for the model-predicted and recorded fatality numbers, respectively, and the absolute errors read as

$$\mathscr{E}_{m,i} = |\Delta F_m(t_i) - \Delta F(t_i)|, \tag{18}$$

if $m = \mathrm{KIN}, \mathrm{KIN2}$, with $\Delta F_m(t_i)$ and $\Delta F(t_i)$ standing for the increments of model-predicted and recorded fatality numbers, respectively. The temporal average reads as

$$\langle \mathscr{E}_m \rangle = \frac{1}{N_i} \sum_{i=1}^{N_i} \mathscr{E}_{m,i}, \tag{19}$$

with $m = \mathrm{HER}, \mathrm{DEL}, \mathrm{KIN}, \mathrm{HER2}, \mathrm{DEL2}, \mathrm{KIN2}$. In more detail, the following optimization problems were solved for each and every of the chosen 102 countries, territories, and US states:

- minimizing the time-averaged absolute error of the kinetics model with one death rate parameter covering the entirety of the investigated pandemic time period, according to

$$\text{minimize} \langle \mathscr{E}_{\mathrm{KIN}}(\beta_{\mathrm{F}}) \rangle \rightarrow \beta_{\mathrm{F}}^{\mathrm{opt}}, \tag{20}$$

  providing 102 country-, territory-, and US-state-specific optimized parameters $\beta_{\mathrm{F}}^{\mathrm{opt}}$;
- minimizing the time-averaged absolute error associated with two, wave-specific, death rate parameters, according to

$$\text{minimize} \langle \mathscr{E}_{\mathrm{KIN2}}(\beta_{\mathrm{F}}^{\mathrm{I}}, \beta_{\mathrm{F}}^{\mathrm{II}}) \rangle \rightarrow \beta_{\mathrm{F}}^{\mathrm{I,opt}}, \beta_{\mathrm{F}}^{\mathrm{II,opt}}, \tag{21}$$

  providing 102 country-, territory-, and US-state-specific optimized parameters $\beta_{\mathrm{F}}^{\mathrm{I,opt}}$, and as many optimized parameters $\beta_{\mathrm{F}}^{\mathrm{II,opt}}$;
- minimizing the time-averaged absolute error of the delay model with one pair of parameters $(f_{\mathrm{F,DEL}}, T_{\mathrm{F,DEL}})$ covering the entirety of the investigated pandemic time period, according to

$$\text{minimize} \langle \mathscr{E}_{\mathrm{DEL}}(f_{\mathrm{F,DEL}}, T_{\mathrm{F,DEL}}) \rangle \rightarrow f_{\mathrm{F,DEL}}^{\mathrm{opt}}, T_{\mathrm{F,DEL}}^{\mathrm{opt}}, \tag{22}$$

  providing 102 country-, territory-, and US-state-specific optimized parameter pairs $(f_{\mathrm{F,DEL}}^{\mathrm{opt}}, T_{\mathrm{F,DEL}}^{\mathrm{opt}})$;

- minimizing the time-averaged absolute error of the delay model with two, wave-specific, pairs of parameters, $(f^{\mathrm{I}}_{\mathrm{F,DEL}}, T^{\mathrm{I}}_{\mathrm{F,DEL}})$ and $(f^{\mathrm{II}}_{\mathrm{F,DEL}}, T^{\mathrm{II}}_{\mathrm{F,DEL}})$, according to

$$\begin{aligned}&\text{minimize}\ \langle \mathscr{E}_{\mathrm{DEL2}}(f^{\mathrm{I}}_{\mathrm{F,DEL}}, T^{\mathrm{I}}_{\mathrm{F,DEL}}, f^{\mathrm{II}}_{\mathrm{F,DEL}}, T^{\mathrm{II}}_{\mathrm{F,DEL}})\rangle \\ &\quad \rightarrow f^{\mathrm{I,opt}}_{\mathrm{F,DEL}}, T^{\mathrm{I,opt}}_{\mathrm{F,DEL}}, f^{\mathrm{II,opt}}_{\mathrm{F,DEL}}, T^{\mathrm{II,opt}}_{\mathrm{F,DEL}},\end{aligned} \tag{23}$$

providing 102 country-, territory-, and US-state-specific optimized parameter pairs $(f^{\mathrm{I,opt}}_{\mathrm{F,DEL}}, T^{\mathrm{I,opt}}_{\mathrm{F,DEL}})$, and as many optimized parameter pairs $(f^{\mathrm{II,opt}}_{\mathrm{F,DEL}}, T^{\mathrm{II,opt}}_{\mathrm{F,DEL}})$;
- minimizing the time-averaged absolute error of the hereditary model with one triple of parameters $(f_{\mathrm{F,HER}}, T_{\mathrm{F,HER}}, s_{\mathrm{HER}})$ covering the entirety of the investigated pandemic time period, according to

$$\begin{aligned}&\text{minimize}\ \langle \mathscr{E}_{\mathrm{HER}}(f_{\mathrm{F,HER}}, T_{\mathrm{F,HER}}, s_{\mathrm{HER}})\rangle \\ &\quad \rightarrow f^{\mathrm{opt}}_{\mathrm{F,HER}}, T^{\mathrm{opt}}_{\mathrm{F,HER}}, s^{\mathrm{opt}}_{\mathrm{HER}},\end{aligned} \tag{24}$$

providing 102 country-, territory-, and US-state-specific optimized parameter triples $(f^{\mathrm{opt}}_{\mathrm{F,HER}}, T^{\mathrm{opt}}_{\mathrm{F,HER}}, s^{\mathrm{opt}}_{\mathrm{HER}})$;
- minimizing the time-averaged absolute error of the hereditary model with two, wave-specific, triples of parameters $(f^{\mathrm{I}}_{\mathrm{F,HER}}, T^{\mathrm{I}}_{\mathrm{F,HER}}, s^{\mathrm{I}}_{\mathrm{HER}})$ and $(f^{\mathrm{II}}_{\mathrm{F,HER}}, T^{\mathrm{II}}_{\mathrm{F,HER}}, s^{\mathrm{II}}_{\mathrm{HER}})$, according to

$$\begin{aligned}&\text{minimize}\ \langle \mathscr{E}_{\mathrm{HER2}}(f^{\mathrm{I}}_{\mathrm{F,HER}}, T^{\mathrm{I}}_{\mathrm{F,HER}}, s^{\mathrm{I}}_{\mathrm{HER}}, f^{\mathrm{II}}_{\mathrm{F,HER}}, T^{\mathrm{II}}_{\mathrm{F,HER}}, s^{\mathrm{II}}_{\mathrm{HER}})\rangle \\ &\quad \rightarrow f^{\mathrm{I,opt}}_{\mathrm{F,HER}}, T^{\mathrm{I,opt}}_{\mathrm{F,HER}}, s^{\mathrm{I,opt}}_{\mathrm{HER}}, f^{\mathrm{II,opt}}_{\mathrm{F,HER}}, T^{\mathrm{II,opt}}_{\mathrm{F,HER}}, s^{\mathrm{II,opt}}_{\mathrm{HER}},\end{aligned} \tag{25}$$

providing 102 country-, territory-, and US-state-specific optimized parameter triples $(f^{\mathrm{I,opt}}_{\mathrm{F,HER}}, T^{\mathrm{I,opt}}_{\mathrm{F,HER}}, s^{\mathrm{I,opt}}_{\mathrm{HER}})$, and as many optimized parameter triples $(f^{\mathrm{II,opt}}_{\mathrm{F,HER}}, T^{\mathrm{II,opt}}_{\mathrm{F,HER}}, s^{\mathrm{II,opt}}_{\mathrm{HER}})$.

Equations (20)–(25) are actually solved by an interior point algorithm,[59–61] which is readily available via the fmincon-function implemented in the Optimization Toolbox of the commercial mathematics software MATLAB.[62] Thereby, we used version 2020b, run on a Linux operating system (Fedora 32—Workstation Edition). Considering earlier experience with the kinetics and the infection-to-death delay model,[55] the following bounds were imposed onto the parameters to be optimized: $0 < \beta^k_{\mathrm{F}} < 0.003$ with $k = \mathrm{I, II}$; $0 < f^k_{\mathrm{F},m} < 0.6$ with $m = \mathrm{DEL, HER}$ and $k = \mathrm{I, II}$; $5\,\mathrm{d} < T^k_{\mathrm{F},m} < 60\,\mathrm{d}$ with $m = \mathrm{DEL, HER}$ and $k = \mathrm{I, II}$; and $s^k_m > 0$ with $m = \mathrm{HER}$ and $k = \mathrm{I, II}$.

We also compare the model performances among each other, by computing relative differences between model prediction errors as

$$\Delta\mathscr{E}_{m-n} = \frac{\langle \mathscr{E}_m\rangle - \langle \mathscr{E}_n\rangle}{\langle \mathscr{E}_n\rangle}, \tag{26}$$

with $m, n = \mathrm{HER, HER2, DEL, DEL2, KIN, KIN2}$. In this context, $\mathscr{E}_{m-n}$ refers to the case when the optimized model parameters cover the entire time period studied, and an additional subscript "2" indicates the use of wave-specifically optimized model parameters.

Finally, the exactness of the model predictions with the optimized parameters is assessed through the coefficient of determination R^2, according to

$$R^2_m = 1 - \left(\frac{\sum_i^{N_i}\left(F(t_i) - F_m(t_i)\right)^2}{\sum_i^{N_i}\left(F(t_i) - \frac{1}{N_i}\sum_i^{N_i} F(t_i)\right)^2}\right), \tag{27}$$

with $m, n = \mathrm{HER, HER2, DEL, DEL2, KIN, KIN2}$; and through normalized time-averaged errors ("relative errors"),

$$\langle \mathscr{R}_m\rangle = \frac{\langle \mathscr{E}_m\rangle}{F_{\max}}, \tag{28}$$

with $m, n = \mathrm{HER, HER2, DEL, DEL2, KIN, KIN2}$, whereby $F_{\max}$ stands for the maximum number of fatalities, that is, the total numbers recorded until December 31, 2020.

IV. RESULTS

For the epidemic model parameters referring to the entirety of the investigated pandemic time period, which spans from February to December 2020, our newly introduced hereditary model outperforms the traditional kinetics model in terms of fatality trend predictions for 101 out of 102 countries, territories, or US states, see Table I, as well as the third column of Table II for model error reductions encountered when comparing the kinetics model with the hereditary model. These reductions reach values as high as 96.4% (in the case of Ghana), and on average, they amount to 64.5%. The superiority of the new modeling approach is even more pronounced in the case of wave-specific parameter optimization, see the sixth column of Table II; for actually all of the investigated countries, territories, and US states, the hereditary model outperforms the kinetics model, with a maximum error reduction of 98.3% (in the case of New Jersey), and the average over all 102 country-, territory-, and US state-specific error reductions amounting to 83.9%. This is consistent with the hereditary model capturing much better the significantly changing epidemic characteristics between the first and the second wave, which can be clearly seen from Fig. 2 and in particular, from Fig. 3. Let us first go into details regarding the Austrian case depicted in Fig. 2. Comparing Figs. 2(c) and 2(e), it is evident that all of the three investigated modeling approaches perform (significantly) better when dividing the studied time domain into a first and a second infection wave. While the deviations between the model-predicted and recorded fatalities are partly significant when considering only one set of model parameters for the whole time domain, see Fig. 2(c), these deviations are clearly reduced when considering infection wave-specific model parameters, and this is particularly true for the hereditary model, as impressively illustrated in Fig. 2(e). From a qualitative point of view, the same findings can be reported for the state of New York, see Fig. 3. However, in this case, the benefits of considering infection wave-specific model parameters are even more pronounced, and particularly striking for the hereditary model. While evaluating the hereditary model with infection wave-specific model parameters yields an extremely good agreement between model-predicted and recorded fatalities over the whole time domain, see Fig. 3(e), evaluating it with model parameters valid for the whole time domain leads to significant deviations, especially for $t > 210$ days. Obviously, this deficit can be attributed to the fact that one set of model parameters cannot satisfyingly represent the relation between confirmed infections and correspondingly arising fatalities over a long period of time (irrespective of the chosen modeling

TABLE I. Optimal parameters covering the entirety of the investigated pandemic time period, for the death kinetics law (β_F^{opt}), for the infection-to-death delay model ($f_{F,DEL}^{opt}$ and $T_{F,DEL}^{opt}$), and for the hereditary model (s_{HER}^{opt}, $f_{F,HER}^{opt}$, and $T_{F,HER}^{opt}$) as well as the corresponding time-averaged absolute errors ($\langle \mathscr{E}_{KIN} \rangle$, $\langle \mathscr{E}_{DEL} \rangle$, $\langle \mathscr{E}_{HER} \rangle$).

Country	β_F^{opt} (10^{-4} d^{-1})	$\langle \mathscr{E}_{KIN} \rangle$ (—)	$f_{F,DEL}^{opt}$ (—)	$T_{F,DEL}^{opt}$ (d)	$\langle \mathscr{E}_{DEL} \rangle$ (—)	s_{HER}^{opt} (d^{-1})	$f_{F,HER}^{opt}$ (—)	$T_{F,HER}^{opt}$ (d)	$\langle \mathscr{E}_{HER} \rangle$ (—)
Afghanistan	8.16	162.51	0.04	19.40	60.53	0.09	0.04	19.07	46.69
Albania	6.16	115.54	0.04	24.80	33.17	0.14	0.04	27.23	32.70
Andorra	0.00	50.79	0.06	58.53	24.33	8.03	0.06	60.00	23.75
Arizona	1.38	2143.82	0.03	15.10	338.52	3.63	0.03	16.03	337.77
Arkansas	15.57	62.08	0.02	26.10	44.64	0.06	0.02	26.77	35.50
Armenia	8.33	67.57	0.02	7.50	53.65	0.07	0.02	10.86	42.45
Australia	11.77	107.42	0.03	26.30	47.30	1.05	0.03	25.82	47.09
Austria	12.93	253.65	0.02	18.60	227.92	0.07	0.04	46.09	162.17
Azerbaijan	8.04	95.70	0.02	8.70	31.56	0.06	0.02	8.89	21.25
Bahrain	3.19	26.04	0.00	12.20	3.94	1.46	0.00	12.55	3.88
Bangladesh	3.83	600.08	0.01	10.10	77.08	0.11	0.01	5.00	64.60
Belarus	3.66	110.76	0.01	18.50	66.79	0.03	0.01	36.77	25.03
Belgium	2.20	7389.85	0.14	58.64	3676.68	>10	0.14	60.00	3526.52
Bolivia	13.39	1004.58	0.06	10.20	55.73	0.11	0.06	6.96	43.98
Bosnia and Herzegovina	14.74	51.74	0.04	14.40	45.88	0.61	0.04	14.44	45.34
Brazil	13.50	27 244.64	0.03	6.00	10 622.69	1.17	0.03	5.00	10 476.22
Bulgaria	14.34	61.52	0.04	14.90	58.65	0.15	0.05	18.55	38.06
California	2.04	5265.39	0.02	12.60	1518.19	>10	0.02	14.02	1512.63
Canada	15.14	3233.87	0.08	49.10	1807.43	3.51	0.08	56.43	1782.96
Chile	24.59	1395.10	0.03	13.70	72.88	>10	0.03	12.93	67.32
China	18.20	1263.72	0.05	12.32	251.68	0.05	0.06	11.37	135.14
Colorado	1.94	1138.63	0.04	48.10	468.02	9.81	0.04	45.99	468.02
Connecticut	2.94	2921.95	0.09	45.70	836.92	>10	0.09	38.15	826.60
Costa Rica	3.78	73.87	0.01	11.50	14.87	2.23	0.01	8.86	11.86
Cote d'Ivoire	0.00	80.44	0.01	6.50	6.66	1.51	0.01	5.00	6.48
Croatia	25.16	115.15	0.02	13.90	32.41	0.15	0.02	18.08	28.93
Czechia	17.98	330.37	0.02	13.00	125.18	0.14	0.02	12.52	108.53
Delaware	1.33	403.38	0.03	18.60	109.12	1.34	0.03	25.51	107.75
Dem. Rep. Congo	5.11	90.86	0.03	6.00	16.45	0.34	0.03	5.00	16.09
Denmark	3.92	433.59	0.04	58.59	214.49	9.36	0.04	60.00	211.65
Dominican Republic	2.89	714.78	0.02	5.99	145.00	0.69	0.02	5.00	143.42
Ecuador	24.41	3118.53	0.08	6.00	1569.36	0.85	0.08	5.00	1556.14
Egypt	12.99	584.30	0.06	12.20	131.77	0.05	0.06	5.00	61.63
El Salvador	9.95	102.44	0.03	6.00	10.88	0.28	0.03	5.00	10.09
Estonia	4.22	27.16	0.03	44.50	11.72	0.28	0.03	45.41	11.62
Eswatini	7.79	17.93	0.02	6.46	2.74	2.28	0.02	5.02	2.70
Finland	2.46	233.24	0.05	58.51	71.99	8.94	0.05	60.00	71.78
France	7.76	21 315.15	0.03	6.01	14 766.54	0.30	0.03	5.00	14 682.89
Germany	10.48	4094.74	0.05	45.80	1408.29	0.17	0.05	46.30	1376.55
Ghana	0.00	179.90	0.01	12.49	7.63	0.10	0.01	7.18	6.45
Greece	24.06	150.02	0.04	21.00	70.25	1.32	0.04	20.23	69.75
Haiti	0.01	142.51	0.03	15.40	8.32	0.06	0.03	5.13	5.90
Hawaii	2.25	54.24	0.02	17.00	7.31	0.08	0.02	20.53	5.68
Hungary	9.27	393.18	0.03	9.20	273.25	0.03	0.08	60.00	204.67
Indonesia	18.00	843.63	0.04	5.99	996.76	1.26	0.03	5.00	988.69
Ireland	1.17	1396.31	0.07	58.53	446.55	>10	0.07	60.00	443.74
Israel	5.30	120.02	0.01	12.90	79.81	0.10	0.01	11.30	59.75

TABLE I. (*Continued.*)

Country	β_F^{opt} (10^{-4} d^{-1})	$\langle \mathscr{E}_{KIN} \rangle$ (—)	$f_{F,DEL}^{opt}$ (—)	$T_{F,DEL}^{opt}$ (d)	$\langle \mathscr{E}_{DEL} \rangle$ (—)	s_{HER}^{opt} (d^{-1})	$f_{F,HER}^{opt}$ (—)	$T_{F,HER}^{opt}$ (d)	$\langle \mathscr{E}_{HER} \rangle$ (—)
Italy	8.90	23 343.57	0.15	56.67	7298.56	2.39	0.15	56.24	7298.84
Kansas	1.60	445.87	0.01	6.00	64.06	0.12	0.01	16.22	59.58
Kazakhstan	8.70	109.36	0.02	22.50	64.25	0.09	0.02	21.97	58.44
Kenya	5.22	141.41	0.02	5.99	35.73	0.35	0.02	5.00	33.80
Kosovo	10.61	163.86	0.04	20.40	59.02	0.08	0.04	29.12	50.89
Malawi	0.00	106.38	0.03	7.42	4.47	>10	0.03	7.00	4.48
Malaysia	2.79	85.91	0.01	44.00	43.33	0.04	0.02	59.98	36.73
Massachusetts	12.89	3860.40	0.08	24.02	1070.64	>10	0.08	27.96	1065.22
Mauritania	9.03	33.54	0.02	6.50	14.33	9.76	0.02	5.00	13.99
Mexico	30.00	25 788.29	0.10	6.00	3956.11	0.00	0.20	5.09	3272.22
Michigan	4.11	4601.48	0.07	56.60	1761.48	>10	0.07	53.07	1755.66
Minnesota	13.60	819.50	0.03	45.50	432.21	7.36	0.03	46.91	430.26
Montenegro	6.57	50.51	0.02	6.00	12.80	0.46	0.02	5.00	12.32
Morocco	16.65	171.88	0.02	6.03	104.91	0.55	0.02	5.00	98.66
Namibia	4.18	13.35	0.01	8.70	3.39	>10	0.01	6.00	3.21
Nebraska	2.59	143.59	0.01	23.60	43.91	0.14	0.01	23.54	41.88
Nepal	7.13	101.66	0.01	8.70	47.69	0.03	0.01	30.38	29.68
New Hampshire	10.67	206.44	0.06	45.30	68.12	>10	0.06	45.10	68.19
New Jersey	4.69	9089.18	0.07	14.50	2277.78	5.46	0.08	21.48	2251.66
New Mexico	4.22	268.90	0.04	34.50	125.46	0.66	0.04	35.42	124.76
New York	2.65	22 331.89	0.07	6.48	4467.88	>10	0.07	5.89	4474.14
Nigeria	3.91	302.88	0.02	5.99	78.11	8.66	0.02	5.00	77.03
North Macedonia	12.98	180.69	0.03	6.49	93.27	0.05	0.05	35.47	73.19
Norway	1.25	174.39	0.03	58.56	56.34	9.88	0.03	60.00	56.11
Ohio	10.07	1714.77	0.04	29.70	823.38	0.15	0.04	34.01	811.88
Oman	4.46	151.06	0.01	31.50	53.46	0.03	0.01	54.21	10.94
Panama	8.05	181.41	0.02	6.00	126.81	9.77	0.02	5.00	125.95
Pakistan	10.54	239.55	0.02	6.01	174.43	>10	0.02	5.00	169.05
Paraguay	7.56	188.68	0.02	6.50	25.58	1.14	0.02	5.00	25.30
Pennsylvania	9.76	2857.13	0.06	41.10	1461.34	>10	0.06	41.00	1461.39
Peru	14.56	7639.74	0.04	6.00	3173.60	1.09	0.04	5.00	3127.06
Poland	12.64	499.77	0.02	10.70	605.27	0.04	0.04	37.92	380.11
Portugal	8.50	397.55	0.03	37.20	352.23	0.06	0.03	44.01	315.79
Qatar	0.57	62.53	0.00	30.80	5.51	0.11	0.00	23.22	2.32
Rhode Island	1.77	605.04	0.05	49.00	189.67	7.48	0.05	45.79	189.27
Romania	14.79	600.12	0.03	6.47	850.67	0.00	0.05	33.18	764.87
Russia	8.47	2638.08	0.02	6.00	664.97	1.12	0.02	5.10	663.64
Senegal	5.90	53.34	0.02	9.50	7.19	0.81	0.02	8.48	7.17
Somalia	0.00	80.48	0.03	6.42	8.73	0.94	0.03	5.00	8.62
South Africa	16.62	498.81	0.03	15.80	775.22	0.03	0.03	7.01	231.02
South Dakota	9.01	31.70	0.02	21.70	12.84	>10	0.02	21.39	12.85
State of Palestine	7.53	83.06	0.01	7.60	17.32	0.37	0.01	5.08	16.79
Sudan	3.96	676.19	0.08	6.48	60.03	2.56	0.08	5.01	59.97
Suriname	10.49	24.03	0.02	10.40	1.82	0.34	0.02	10.01	1.78
Switzerland	8.99	1008.01	0.06	57.70	548.10	0.07	0.06	60.00	469.10
Tennessee	8.41	265.40	0.01	6.50	98.78	0.04	0.02	15.97	61.07
Texas	7.24	1325.58	0.02	14.50	578.44	7.52	0.02	13.86	578.32
Turkey	13.11	488.97	0.01	6.00	373.10	0.28	0.01	5.00	355.55

TABLE I. (*Continued.*)

Country	β_F^{opt} (10^{-4} d^{-1})	$\langle \mathscr{E}_{KIN} \rangle$ (—)	$f_{F,DEL}^{opt}$ (—)	$T_{F,DEL}^{opt}$ (d)	$\langle \mathscr{E}_{DEL} \rangle$ (—)	s_{HER}^{opt} (d^{-1})	$f_{F,HER}^{opt}$ (—)	$T_{F,HER}^{opt}$ (d)	$\langle \mathscr{E}_{HER} \rangle$ (—)
United Arab Emirates	1.51	141.56	0.00	6.47	75.71	0.58	0.00	5.00	75.43
Utah	2.03	122.11	0.01	48.00	61.54	4.24	0.01	49.40	61.33
Uzbekistan	6.78	58.92	0.01	14.20	12.51	0.88	0.01	12.28	12.19
Virginia	1.19	1353.94	0.02	5.99	377.81	7.95	0.02	5.00	377.83
Wisconsin	8.23	235.32	0.01	5.50	268.78	0.03	0.01	20.74	253.41
Zambia	7.08	140.03	0.02	6.47	22.41	1.58	0.02	5.00	22.04
Zimbabwe	6.64	70.91	0.03	9.49	5.51	1.12	0.03	7.84	5.45

TABLE II. Relative differences between model-specific prediction errors according to Eq. (26), for parameters optimized over the entire investigated pandemic time period, and for wave-specific parameters (indicated by subscript 2).

Country	$\Delta\mathscr{E}_{DEL-KIN}$ (—)	$\Delta\mathscr{E}_{HER-KIN}$ (—)	$\Delta\mathscr{E}_{HER-DEL}$ (—)	$\Delta\mathscr{E}_{DEL2-KIN2}$ (—)	$\Delta\mathscr{E}_{HER2-KIN2}$ (—)	$\Delta\mathscr{E}_{HER2-DEL2}$ (—)
Afghanistan	−0.6275	−0.7127	−0.2287	−0.7389	−0.8938	−0.5934
Albania	−0.7129	−0.7170	−0.0142	−0.7436	−0.8749	−0.5122
Andorra	−0.5211	−0.5324	−0.0237	0.1773	−0.9039	−0.9184
Arizona	−0.8421	−0.8424	−0.0022	−0.8933	−0.9247	−0.2942
Arkansas	−0.2809	−0.4281	−0.2047	−0.7375	−0.7365	0.0036
Armenia	−0.2060	−0.3717	−0.2086	−0.2124	−0.8608	−0.8233
Australia	−0.5597	−0.5616	−0.0045	−0.6175	−0.9182	−0.7861
Austria	−0.1014	−0.3606	−0.2885	0.0197	−0.6599	−0.6665
Azerbaijan	−0.6703	−0.7780	−0.3267	−0.4034	−0.8469	−0.7435
Bahrain	−0.8488	−0.8509	−0.0141	−0.8504	−0.8545	−0.0275
Bangladesh	−0.8716	−0.8923	−0.1619	−0.8971	−0.9017	−0.0439
Belarus	−0.3970	−0.7741	−0.6253	−0.7525	−0.9509	−0.8014
Belgium	−0.5025	−0.5228	−0.0408	−0.6541	−0.9637	−0.8950
Bolivia	−0.9445	−0.9562	−0.2109	−0.9398	−0.9591	−0.3205
Bosnia and Herzegovina	−0.1132	−0.1236	−0.0118	−0.5737	−0.7271	−0.3599
Brazil	−0.6101	−0.6155	−0.0138	−0.5854	−0.6269	−0.1001
Bulgaria	−0.0465	−0.3812	−0.3510	0.1871	−0.3675	−0.4672
California	−0.7117	−0.7127	−0.0037	−0.7154	−0.6363	0.2779
Canada	−0.4411	−0.4487	−0.0135	−0.1926	−0.9125	−0.8916
Chile	−0.9478	−0.9517	−0.0763	−0.9620	−0.9661	−0.1072
China	−0.8008	−0.8931	−0.4631	−0.9020	−0.9315	−0.3011
Colorado	−0.5890	−0.5890	0.0000	−0.5518	−0.9555	−0.9007
Connecticut	−0.7136	−0.7171	−0.0123	−0.9040	−0.9725	−0.7130
Costa Rica	−0.7988	−0.8395	−0.2025	−0.8101	−0.8593	−0.2590
Cote d'Ivoire	−0.9172	−0.9195	−0.0269	−0.8282	−0.8309	−0.0158
Croatia	−0.7185	−0.7487	−0.1074	−0.7259	−0.8387	−0.4116
Czechia	−0.6211	−0.6715	−0.1330	−0.6675	−0.7607	−0.2802
Delaware	−0.7295	−0.7329	−0.0125	−0.5363	−0.9404	−0.8714
Dem. Rep. Congo	−0.8190	−0.8229	−0.0217	−0.8351	−0.8446	−0.0574
Denmark	−0.5053	−0.5119	−0.0132	0.8680	−0.6938	−0.8361
Dominican Republic	−0.7971	−0.7993	−0.0109	−0.7453	−0.7755	−0.1185
Ecuador	−0.4968	−0.5010	−0.0084	−0.5079	−0.9605	−0.9196
Egypt	−0.7745	−0.8945	−0.5323	−0.9048	−0.9330	−0.2959
El Salvador	−0.8938	−0.9015	−0.0725	−0.8901	−0.9373	−0.4293

TABLE II. (*Continued.*)

Country	$\Delta\mathscr{E}_{\mathrm{DEL-KIN}}$ (—)	$\Delta\mathscr{E}_{\mathrm{HER-KIN}}$ (—)	$\Delta\mathscr{E}_{\mathrm{HER-DEL}}$ (—)	$\Delta\mathscr{E}_{\mathrm{DEL2-KIN2}}$ (—)	$\Delta\mathscr{E}_{\mathrm{HER2-KIN2}}$ (—)	$\Delta\mathscr{E}_{\mathrm{HER2-DEL2}}$ (—)
Estonia	−0.5684	−0.5720	−0.0083	−0.9086	−0.9302	−0.2366
Eswatini	−0.8472	−0.8495	−0.0149	−0.8388	−0.8902	−0.3187
Finland	−0.6913	−0.6922	−0.0029	−0.6570	−0.9046	−0.7218
France	−0.3072	−0.3112	−0.0057	−0.4326	−0.9661	−0.9402
Germany	−0.6561	−0.6638	−0.0225	−0.3079	−0.6724	−0.5267
Ghana	−0.9576	−0.9641	−0.1544	−0.9648	−0.9738	−0.2573
Greece	−0.5318	−0.5350	−0.0070	−0.5869	−0.6371	−0.1213
Haiti	−0.9416	−0.9586	−0.2908	−0.8877	−0.9284	−0.3624
Hawaii	−0.8652	−0.8953	−0.2237	−0.8622	−0.9459	−0.6075
Hungary	−0.3050	−0.4794	−0.2510	−0.1328	−0.7747	−0.7403
Indonesia	0.1815	0.1719	−0.0081	−0.0916	−0.1498	−0.0640
Ireland	−0.6802	−0.6822	−0.0063	−0.6131	−0.9686	−0.9187
Israel	−0.3350	−0.5022	−0.2514	−0.4314	−0.8981	−0.8207
Italy	−0.6873	−0.6873	0.0000	−0.8487	−0.9806	−0.8716
Kansas	−0.8563	−0.8664	−0.0700	−0.8860	−0.9086	−0.1985
Kazakhstan	−0.4125	−0.4656	−0.0904	−0.5086	−0.6280	−0.2430
Kenya	−0.7473	−0.7610	−0.0539	−0.7893	−0.8673	−0.3704
Kosovo	−0.6398	−0.6894	−0.1377	1.3136	−0.3554	−0.7214
Malawi	−0.9580	−0.9579	0.0020	−0.9618	−0.9607	0.0303
Malaysia	−0.4956	−0.5724	−0.1523	−0.4420	−0.8200	−0.6774
Massachusetts	−0.7227	−0.7241	−0.0051	−0.7295	−0.8083	−0.2913
Mauritania	−0.5728	−0.5830	−0.0238	−0.8151	−0.8315	−0.0886
Mexico	−0.8466	−0.8731	−0.1729	−0.9200	−0.9634	−0.5428
Michigan	−0.6172	−0.6185	−0.0033	0.0155	−0.9134	−0.9147
Minnesota	−0.4726	−0.4750	−0.0045	−0.5130	−0.9364	−0.8694
Montenegro	−0.7466	−0.7560	−0.0371	−0.7668	−0.9359	−0.7250
Morocco	−0.3897	−0.4260	−0.0595	−0.5955	−0.6649	−0.1716
Namibia	−0.7459	−0.7595	−0.0537	−0.7513	−0.7925	−0.1658
Nebraska	−0.6942	−0.7083	−0.0461	−0.7355	−0.9048	−0.6400
Nepal	−0.5309	−0.7080	−0.3776	−0.2002	−0.7372	−0.6714
New Hampshire	−0.6700	−0.6697	0.0010	−0.3781	−0.8370	−0.7379
New Jersey	−0.7494	−0.7523	−0.0115	−0.8683	−0.9831	−0.8720
New Mexico	−0.5334	−0.5360	−0.0056	−0.7241	−0.8284	−0.3781
New York	−0.7999	−0.7997	0.0014	−0.9104	−0.9805	−0.7819
Nigeria	−0.7421	−0.7457	−0.0138	−0.8234	−0.8167	0.0384
North Macedonia	−0.4838	−0.5950	−0.2153	−0.5260	−0.8567	−0.6977
Norway	−0.6769	−0.6783	−0.0041	−0.8498	−0.9542	−0.6948
Ohio	−0.5198	−0.5265	−0.0140	−0.1078	−0.9288	−0.9202
Oman	−0.6461	−0.9275	−0.7953	−0.6889	−0.9574	−0.8632
Panama	−0.3010	−0.3057	−0.0068	−0.7505	−0.7992	−0.1952
Pakistan	−0.2718	−0.2943	−0.0309	−0.8555	−0.8769	−0.1481
Paraguay	−0.8644	−0.8659	−0.0108	−0.5704	−0.8187	−0.5779
Pennsylvania	−0.4885	−0.4885	0.0000	1.8014	−0.7414	−0.9077
Peru	−0.5846	−0.5907	−0.0147	−0.4176	−0.9231	−0.8680
Poland	0.2111	−0.2394	−0.3720	−0.0705	−0.8477	−0.8361
Portugal	−0.1140	−0.2057	−0.1035	−0.3837	−0.9205	−0.8710
Qatar	−0.9119	−0.9628	−0.5781	−0.9185	−0.9704	−0.6372
Rhode Island	−0.6865	−0.6872	−0.0021	−0.7136	−0.9552	−0.8435

TABLE II. (*Continued.*)

Country	$\Delta\mathscr{E}_{\mathrm{DEL-KIN}}$ (—)	$\Delta\mathscr{E}_{\mathrm{HER-KIN}}$ (—)	$\Delta\mathscr{E}_{\mathrm{HER-DEL}}$ (—)	$\Delta\mathscr{E}_{\mathrm{DEL2-KIN2}}$ (—)	$\Delta\mathscr{E}_{\mathrm{HER2-KIN2}}$ (—)	$\Delta\mathscr{E}_{\mathrm{HER2-DEL2}}$ (—)
Romania	0.4175	0.2745	−0.1009	1.4254	−0.7277	−0.8877
Russia	−0.7479	−0.7484	−0.0020	−0.7220	−0.9369	−0.7731
Senegal	−0.8653	−0.8656	−0.0028	−0.8579	−0.8890	−0.2189
Somalia	−0.8916	−0.8929	−0.0119	−0.9305	−0.9316	−0.0164
South Africa	0.5541	−0.5369	−0.7020	0.1877	−0.6204	−0.6804
South Dakota	−0.5948	−0.5945	0.0007	−0.8607	−0.8598	0.0068
State of Palestine	−0.7915	−0.7978	−0.0306	−0.4876	−0.7797	−0.5701
Sudan	−0.9112	−0.9113	−0.0010	−0.9362	−0.9630	−0.4201
Suriname	−0.9242	−0.9258	−0.0210	−0.9230	−0.9260	−0.0390
Switzerland	−0.4563	−0.5346	−0.1441	0.0261	−0.6698	−0.6782
Tennessee	−0.6278	−0.7699	−0.3817	−0.7386	−0.8066	−0.2602
Texas	−0.5636	−0.5637	−0.0002	−0.4128	−0.5862	−0.2954
Turkey	−0.2370	−0.2729	−0.0471	−0.4293	−0.7325	−0.5312
United Arab Emirates	−0.4652	−0.4671	−0.0037	−0.7112	−0.8757	−0.5696
Utah	−0.4960	−0.4978	−0.0035	−0.6203	−0.7828	−0.4278
Uzbekistan	−0.7877	−0.7931	−0.0256	−0.8168	−0.8527	−0.1960
Virginia	−0.7210	−0.7209	0.0001	−0.6689	−0.9234	−0.7686
Wisconsin	0.1422	0.0769	−0.0572	1.1242	−0.5304	−0.7789
Zambia	−0.8399	−0.8426	−0.0165	−0.8774	−0.8663	0.0903
Zimbabwe	−0.9223	−0.9231	−0.0114	−0.9243	−0.9279	−0.0472

approach), at least when this period comprises different pandemic waves. As a rule, the fatality fraction decreases with progression from the first to the second wave (this statement holds for 69 out of the 102 investigated countries, territories, and US states, see columns eleven and fourteen of Table III), and the characteristic time of fatal illness is, as a rule, larger in the second wave when compared to the first wave (this statement holds for 62 out of the 102 investigated countries, territories, and US states, see columns twelve and fifteen of Table III). The superior performance of the hereditary model is also underlined by very low relative predictions errors (see the last column of Table IV). The minimum amounts to 0.11% (in the case of Russia), the maximum does not exceed 5.3% (in the case of Zambia), and the relative average prediction error amounts to 1.2%. Similarly impressive are the coefficients of determination characterizing the fitting procedures (see the seventh column of Table V): the minimum still amounting to 93.5% (in the case of Somalia), the maximum reaching 100.0% (in the case of Russia), and the average over all 102 countries, territories, and US states amounting to 99.3%.

The superiority of the hereditary model with respect to the delay model is less pronounced when determining optimized model parameters for the entirety of the investigated time period, with virtually no such superiority observed for the following countries, territories, or US states (see fourth column of Table II): Arizona, Australia, California, Colorado, Finland, Italy, Malawi, Michigan, Minnesota, New Hampshire, New York, Norway, Pennsylvania, Rhode Island, Russia, Senegal, Somalia, South Dakota, Sudan, Texas, United Arab Emirates, Utah, and Virginia. The latter observation is evident in Fig. 3(c) where the graph representing the delay model (applied to the state of New York) virtually falls together with the graph representing the hereditary model. However, these cases are, on average, characterized by normalized time-averaged errors, which are still as high as 7.13% for the delay model and 7.11% for the hereditary model; and these errors are significantly reduced through splitting the investigated pandemic time period into two, wave-specific, portions, namely, to 3.57% for the delay model, and further down to 1.31% for the hereditary model. This again underlines the superiority of the hereditary model, while the total-number-of-cases-dependent delay model exhibits unrealistic kinks at the wave transition point t_{wtr} (see, e.g., Figs. 2(e) and 3(e)). The hereditary model with two triples of optimized parameters is particularly suitable for countries or US states with two distinctively developed infection waves, irrespective of whether these waves are of very different size (as is the case with Austria, see Fig. 2) or of similar size (as is the case with New York, see Fig. 3). Resting on the increment of confirmed cases, it is also very stable with respect to data inaccuracies, as observed, for example, with the number of recoveries in the case of Norway, which was heavily corrected 86 days after the onset of COVID-19 infections, see the supplementary material. Under these conditions, the traditional kinetics model, building on the number of active infections (which depends on the recorded recoveries) cannot reach a Norway-specific mean relative model error below some 40%, see the ninth column of Table IV. By comparison, the wave-specific use of the hereditary model in the context of Norway yields a normalized time-averaged model error, which is as low as 1.4%, see the fourteenth column of Table IV.

We also take note of the cases where the recorded data virtually turn the general fatality function given by Eq. (5) into the Heaviside format, see Eq. (13), that is, when the fitting procedure yields very high values of s_m, with $m = \mathrm{HER}, \mathrm{HER2}$. This is true for the following countries, territories, or US states (see Tables I and III): Andorra, Bahrain, Canada, China, Cote d'Ivoire, Delaware, Democratic

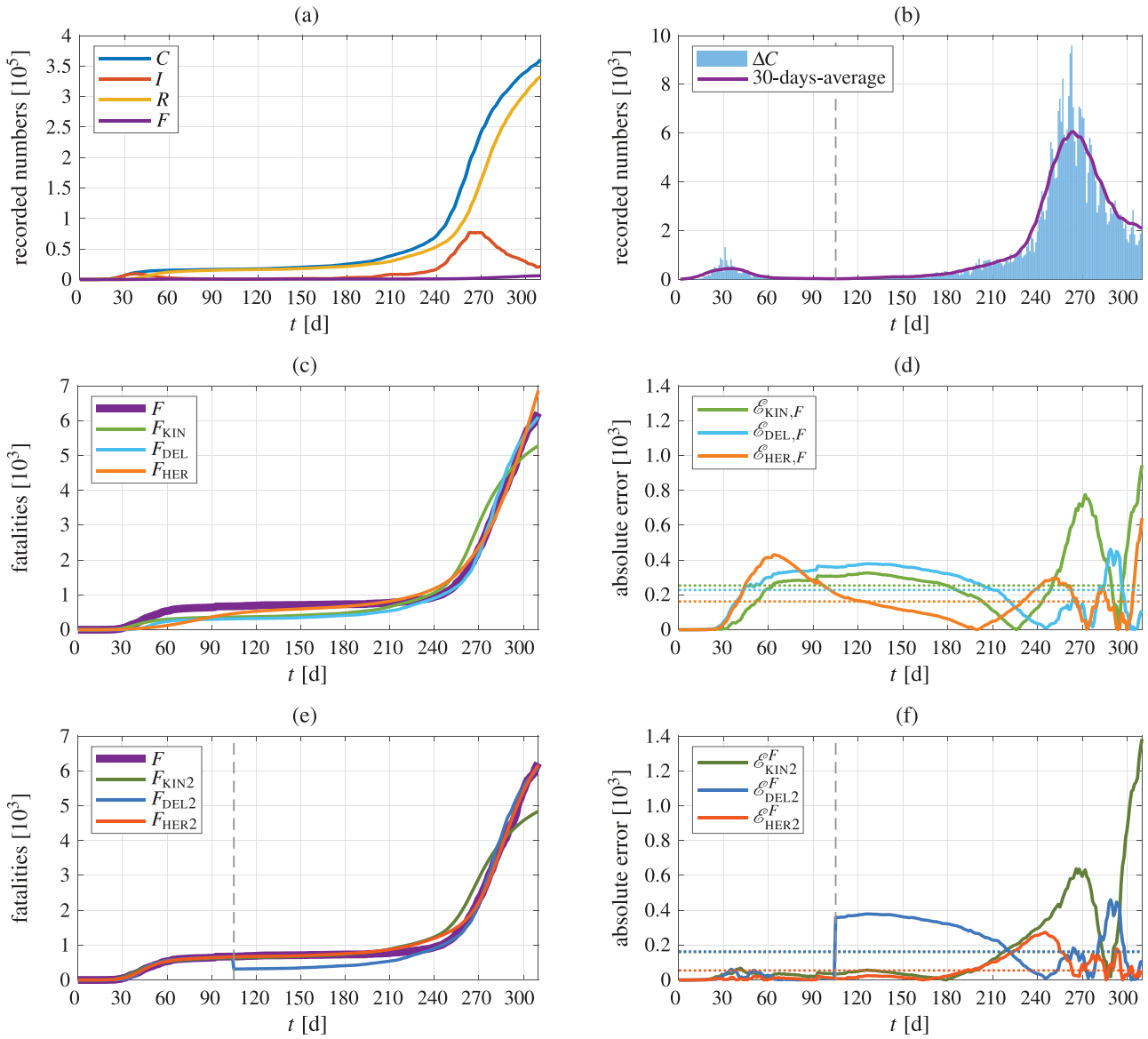

FIG. 2. Data related to Austria, comprising (a) recorded data; (b) daily increments of confirmed cases, ΔC, and their 30 days average; (c) comparison between recorded fatalities and corresponding kinetics, delay, and hereditary model predictions based on parameters optimized for the entirety of the investigated pandemic time period; (d) absolute model errors associated with parameters optimized for the entirety of the investigated pandemic time period; (e) comparison between recorded fatalities and corresponding kinetics, delay, and hereditary model predictions based on wave-specifically optimized parameters, with the wave transition time amounting to $t_{\mathrm{wtr}} = 105$ d; (f) absolute model errors associated with wave-specifically optimized parameters.

Republic of Congo, Estonia, Eswatini, Finland, Greece, Hawaii, Kosovo, Namibia, New Hampshire, Paraguay, Rhode Island, Somalia, South Dakota, and Utah. Still, the differences between the corresponding errors of the hereditary model, see Eqs. (4) and (6)–(11), and errors of the delay model, see Eq. (14), remain, as a rule, significant (see Table II), as the incremental format of the hereditary model (4) differs fundamentally from the simplified total-number-based format of the delay model (14).

V. DISCUSSION AND CONCLUSIONS

While the drawbacks of traditional compartmental SIR modeling have normally motivated "microscopic" agent-based approaches,[10–12] the present contribution followed a different path: not abolishing, but modifying the governing equations for infected, recovered, or deceased persons in an epidemic population. This quest for "new" equations was met by resorting to a mathematical concept, which was very successful in the context of continuum mechanics: integrodifferential

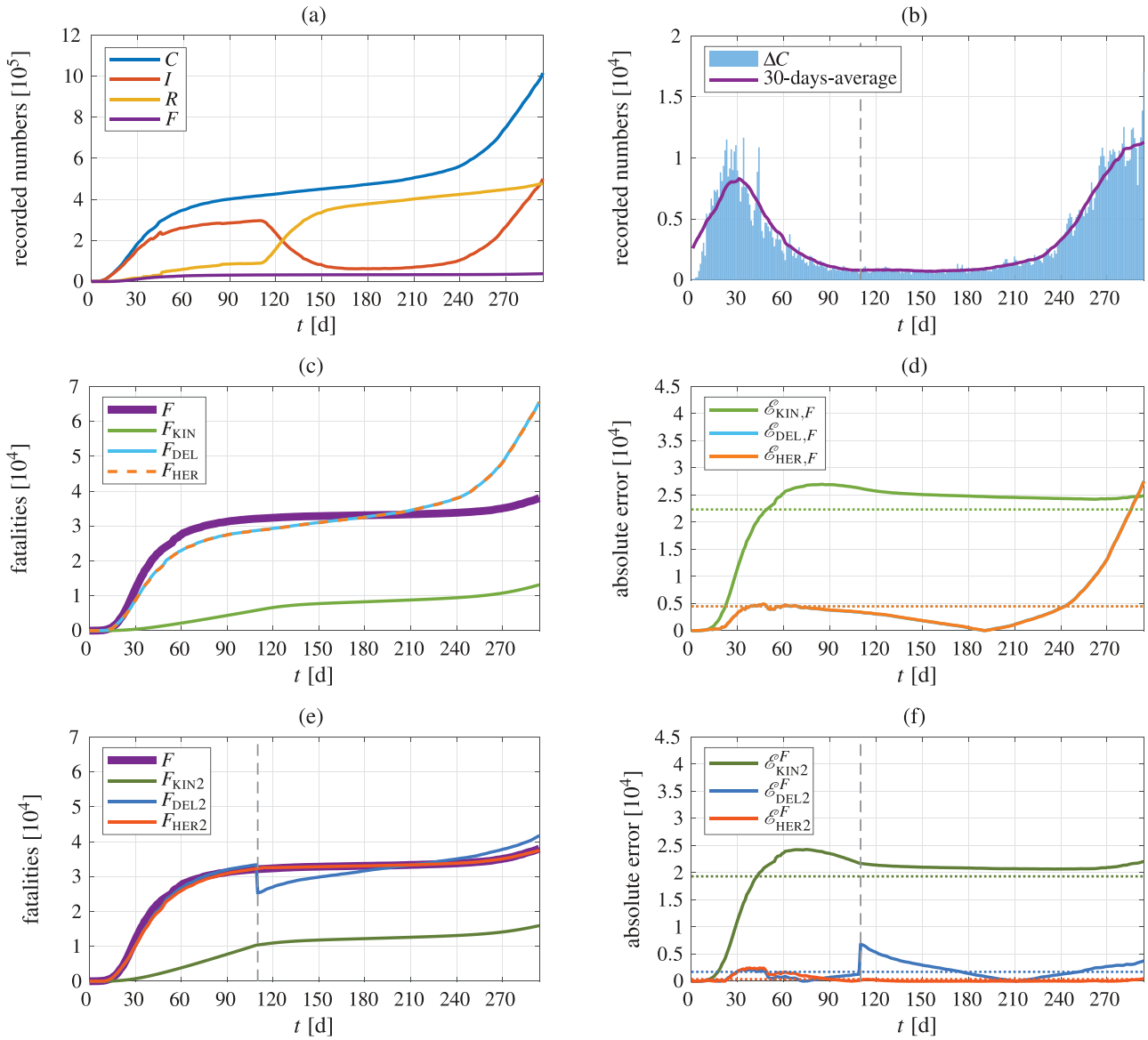

FIG. 3. Data related to New York, comprising (a) recorded data; (b) daily increments of confirmed cases, ΔC, and their 30 days average; (c) comparison between recorded fatalities and corresponding kinetics, delay, and hereditary model predictions based on parameters optimized for the entirety of the investigated pandemic time period; (d) absolute model errors associated with parameters optimized for the entirety of the investigated pandemic time period; (e) comparison between recorded fatalities and corresponding kinetics, delay, and hereditary model predictions based on wave-specifically optimized parameters, with the wave transition time amounting to $t_{wtr} = 110$ d; (f) absolute model errors associated with wave-specifically optimized parameters.

equations proposed by Boltzmann for the "deformation aftereffect" in 1874.[63,64] This adds a new conceptual dimension to disease modeling, regarding the infection-to-death transition not so much as a statistical process, but as a "pseudo-mechanical phenomenon." In this context, the "pseudo-mechanical system" (i.e., the population undergoing the pandemic) is subjected to virus loads developing over time (in terms of the new infections spreading within this population), with these loads leading, in a delayed and convolution-type fashion, to "mechanical strains" (in terms of virus-induced fatalities). In other words, the system partially complies, concedes, or gives up with respect to the virus load, and it is this type of concession or compliance, which drives the fatality trends—quantified here through a logistic function reflecting the corresponding "mechanical creep"; that is, the way the system reacts to the "mechanical" virus load imposed at some past time instant. This particular choice allows for very precisely capturing the fatality trends in 102 countries, territories, and US states, as underlined by coefficients of determination between model predictions and recorded fatalities ranging from 94% to 100%. To the best

TABLE III. Wave-specific optimal parameters for the death kinetics law ($\beta_F^{I,opt}$ and $\beta_F^{II,opt}$), for the infection-to-death delay model ($f_{F,DEL}^{I,opt}$, $f_{F,DEL}^{II,opt}$, $T_{F,DEL}^{I,opt}$, and $T_{F,DEL}^{II,opt}$), and for the hereditary model ($s_{HER}^{I,opt}$, $s_{HER}^{II,opt}$, $f_{F,HER}^{I,opt}$, $f_{F,HER}^{II,opt}$, $T_{F,HER}^{I,opt}$, and $T_{F,HER}^{II,opt}$) as well as the corresponding time-averaged absolute errors ($\langle \mathscr{E}_{KIN2} \rangle$, $\langle \mathscr{E}_{DEL2} \rangle$, $\langle \mathscr{E}_{HER2} \rangle$).

Country	$\beta_F^{I,opt}$ (10^{-4} d^{-1})	$\beta_F^{II,opt}$ (10^{-4} d^{-1})	$\langle \mathscr{E}_{KIN2} \rangle$ (—)	$f_{F,DEL}^{I,opt}$ (—)	$T_{F,DEL}^{I,opt}$ (d)	$f_{F,DEL}^{II,opt}$ (—)	$T_{F,DEL}^{II,opt}$ (d)	$\langle \mathscr{E}_{DEL2} \rangle$ (—)	$s_{HER}^{I,opt}$ (d^{-1})	$f_{F,HER}^{I,opt}$ (—)	$T_{F,HER}^{I,opt}$ (d)	$s_{HER}^{II,opt}$ (d^{-1})	$f_{F,HER}^{II,opt}$ (—)	$T_{F,HER}^{II,opt}$ (d)	$\langle \mathscr{E}_{HER2} \rangle$ (—)
Afghanistan	7.91	9.65	169.79	0.04	20.23	0.04	6.00	44.34	0.11	0.04	18.35	0.08	0.10	29.16	18.03
Albania	0.01	6.16	121.44	0.05	6.49	0.04	24.80	31.14	0.03	0.14	59.85	0.09	0.02	14.48	15.19
Andorra	22.62	0.00	15.95	0.06	8.50	0.06	58.50	18.78	>10	0.07	10.00	9.14	0.00	5.07	1.53
Arizona	2.27	1.38	1555.91	0.03	9.30	0.03	34.20	165.95	0.06	0.03	5.42	0.14	0.02	22.79	117.13
Arkansas	10.79	16.16	120.54	0.01	6.00	0.02	30.20	31.64	0.06	0.02	25.78	0.22	0.02	18.41	31.76
Armenia	9.05	8.04	40.27	0.02	6.48	0.02	9.90	31.71	>10	0.02	7.00	0.09	0.02	12.85	5.60
Australia	6.38	13.64	85.24	0.01	12.50	0.03	26.40	32.61	0.16	0.01	11.51	1.99	0.04	20.11	6.98
Austria	22.54	11.06	160.33	0.04	12.70	0.02	19.10	163.49	0.25	0.04	12.26	0.20	0.02	24.25	54.53
Azerbaijan	9.88	7.74	44.02	0.02	6.46	0.02	10.50	26.26	0.31	0.02	5.43	0.02	0.02	8.52	6.74
Bahrain	2.90	3.82	25.04	0.00	13.49	0.00	13.10	3.75	>10	0.00	11.03	>10	0.00	14.00	3.64
Bangladesh	3.91	3.13	610.18	0.01	6.00	0.01	10.20	62.76	0.11	0.01	5.00	0.02	0.03	59.13	60.00
Belarus	2.63	3.98	187.86	0.01	10.41	0.01	45.40	46.49	0.02	0.01	55.25	0.01	0.01	33.45	9.23
Belgium	9.78	2.19	5976.70	0.17	6.48	0.14	58.55	2067.41	>10	0.16	5.00	0.14	0.02	20.93	217.02
Bolivia	14.27	4.14	829.27	0.06	10.20	0.06	30.80	49.94	0.09	0.06	5.14	0.00	0.02	33.76	33.94
Bosnia and Herzegovina	12.80	15.03	92.16	0.03	6.43	0.04	15.80	39.29	0.01	0.06	39.89	0.15	0.04	16.53	25.15
Brazil	15.65	10.74	19 821.18	0.03	6.00	0.03	51.20	8218.72	0.87	0.03	5.00	>10	0.01	6.35	7396.08
Bulgaria	16.12	14.16	42.20	0.04	6.46	0.04	15.00	50.09	0.06	0.05	10.19	0.23	0.04	16.32	26.69
California	3.56	1.65	2682.75	0.02	6.00	0.02	30.90	763.62	>10	0.02	14.96	>10	0.01	14.87	975.79
Canada	29.72	13.32	855.03	0.09	10.30	0.08	59.01	690.36	7.99	0.09	8.04	0.83	0.02	20.64	74.84
Chile	22.76	30.00	1789.07	0.03	13.50	0.03	29.60	67.90	>10	0.03	12.15	>10	0.03	12.87	60.62
China	18.29	0.00	1384.12	0.04	6.50	0.06	40.57	135.60	0.05	0.06	13.49	>10	0.00	6.00	94.78
Colorado	7.70	1.94	598.74	0.06	6.48	0.04	51.70	268.34	>10	0.06	5.00	1.00	0.01	15.88	26.66
Connecticut	8.36	2.44	1948.87	0.09	5.49	0.09	58.51	187.05	>10	0.09	5.87	>10	0.03	38.14	53.68
Costa Rica	0.00	3.78	78.17	0.02	23.31	0.01	11.50	14.85	>10	0.01	7.88	1.68	0.01	8.56	11.00
Cote d'Ivoire	1.70	0.00	37.77	0.01	6.50	0.01	6.47	6.49	7.00	0.01	5.00	>10	0.00	11.00	6.39
Croatia	16.19	25.16	95.93	0.05	18.50	0.02	13.90	26.30	0.23	0.05	16.88	0.30	0.02	16.32	15.47
Czechia	19.24	17.84	331.05	0.04	10.40	0.02	13.10	110.06	>10	0.03	8.00	0.14	0.02	13.16	79.22
Delaware	14.75	1.18	169.97	0.04	6.40	0.04	59.00	78.81	0.07	0.05	7.19	>10	0.02	31.00	10.14
Dem. Rep. Congo	5.11	10.45	87.08	0.03	6.50	0.03	6.50	14.36	0.41	0.03	5.01	>10	0.06	12.00	13.53
Denmark	30.00	3.87	56.64	0.05	6.46	0.04	58.52	105.80	8.96	0.05	5.01	0.04	0.01	59.92	17.34
Dominican Republic	4.89	0.88	413.56	0.02	6.00	0.02	32.71	105.34	0.51	0.02	5.00	>10	0.00	22.63	92.86
Ecuador	30.00	23.01	3029.74	0.14	8.50	0.08	6.00	1490.89	0.03	0.26	21.53	0.11	0.03	5.00	119.80
Egypt	11.61	27.53	844.86	0.05	10.10	0.06	8.60	80.44	0.06	0.06	5.00	0.00	0.09	32.12	56.64
El Salvador	7.76	12.15	158.50	0.03	6.46	0.04	45.70	17.42	0.25	0.03	5.00	0.27	0.03	5.01	9.94
Estonia	0.00	4.22	51.43	0.03	11.20	0.03	42.70	4.70	>10	0.03	9.00	0.06	0.02	41.18	3.59
Eswatini	7.10	16.92	20.11	0.02	7.49	0.02	58.50	3.24	2.31	0.02	5.39	>10	0.12	31.95	2.21

TABLE III. (*Continued.*)

Country	$\beta_F^{I,opt}$ (10^{-4} d^{-1})	$\beta_F^{II,opt}$ (10^{-4} d^{-1})	$\langle \mathscr{E}_{KIN2} \rangle$ (—)	$f_{F,DEL}^{I,opt}$ (—)	$T_{F,DEL}^{I,opt}$ (d)	$f_{F,DEL}^{II,opt}$ (—)	$T_{F,DEL}^{II,opt}$ (d)	$\langle \mathscr{E}_{DEL2} \rangle$ (—)	$s_{HER}^{I,opt}$ (d^{-1})	$f_{F,HER}^{I,opt}$ (—)	$T_{F,HER}^{I,opt}$ (d)	$s_{HER}^{II,opt}$ (d^{-1})	$f_{F,HER}^{II,opt}$ (—)	$T_{F,HER}^{II,opt}$ (d)	$\langle \mathscr{E}_{HER2} \rangle$ (—)
Finland	19.53	0.00	78.92	0.05	6.20	0.04	58.51	27.07	>10	0.05	5.50	8.94	0.02	60.00	7.53
France	30.00	6.83	17 462.61	0.21	6.50	0.10	59.00	9908.80	>10	0.20	5.00	0.13	0.02	26.07	592.16
Germany	28.27	9.16	887.36	0.05	13.82	0.05	45.60	614.16	0.31	0.05	12.89	7.02	0.03	33.74	290.67
Ghana	0.00	0.00	179.91	0.01	12.38	0.01	48.12	6.34	0.07	0.01	5.11	0.01	0.00	32.51	4.71
Greece	30.00	24.06	145.40	0.06	6.70	0.04	21.10	60.06	>10	0.06	8.00	1.62	0.04	20.62	52.77
Haiti	3.13	0.01	69.26	0.03	12.50	0.03	52.80	7.78	0.06	0.03	5.13	>10	0.34	53.97	4.96
Hawaii	3.15	0.00	50.14	0.01	15.30	0.02	30.49	6.91	>10	0.03	9.93	0.09	0.02	23.87	2.71
Hungary	30.00	9.14	213.06	0.14	8.49	0.03	10.70	184.77	0.00	0.27	32.86	0.07	0.04	26.81	47.99
Indonesia	18.46	17.11	748.48	0.04	5.99	0.05	43.20	679.91	0.63	0.04	5.00	>10	0.03	14.03	636.37
Ireland	30.00	1.10	474.73	0.07	7.00	0.07	58.51	183.69	>10	0.07	7.08	0.04	0.01	34.13	14.93
Israel	6.78	5.17	118.23	0.02	9.50	0.01	13.20	67.22	>10	0.02	10.99	0.11	0.01	14.91	12.05
Italy	30.00	8.75	12 006.31	0.15	6.43	0.15	58.51	1816.28	0.71	0.15	5.00	0.21	0.02	16.49	233.24
Kansas	5.68	1.12	431.26	0.03	6.48	0.02	20.80	49.18	8.92	0.02	5.00	0.13	0.01	20.25	39.42
Kazakhstan	9.08	6.46	132.27	0.02	19.80	0.02	33.70	64.99	0.19	0.02	22.35	0.00	0.02	34.41	49.20
Kenya	4.47	5.59	165.44	0.02	6.48	0.02	6.48	34.86	0.01	0.03	5.21	0.78	0.01	5.00	21.95
Kosovo	22.16	10.01	16.03	0.04	14.47	0.05	33.51	37.08	>10	0.04	11.00	0.20	0.02	6.46	10.33
Malawi	0.00	0.00	106.38	0.03	6.42	0.03	20.20	4.06	1.98	0.03	5.52	>10	0.00	6.00	4.18
Malaysia	5.67	2.62	53.05	0.02	6.50	0.01	42.90	29.60	0.00	0.03	32.05	0.00	0.01	32.72	9.55
Massachusetts	26.53	8.08	1049.05	0.08	10.90	0.08	59.00	283.80	>10	0.08	13.49	>10	0.06	50.09	201.13
Mauritania	3.83	20.29	74.44	0.02	6.48	0.02	6.48	13.76	9.76	0.02	5.00	9.94	0.03	7.29	12.55
Mexico	30.00	30.00	25 788.21	0.12	6.47	0.12	31.49	2062.82	0.00	0.21	33.67	0.00	0.13	29.07	943.14
Michigan	30.00	4.00	841.48	0.10	6.20	0.07	59.01	854.56	>10	0.09	5.00	0.52	0.02	14.65	72.86
Minnesota	30.00	12.22	601.83	0.05	6.01	0.04	55.50	293.12	8.01	0.05	5.00	0.12	0.01	14.57	38.29
Montenegro	6.40	6.63	50.37	0.02	6.50	0.02	6.48	11.74	0.04	0.03	18.76	0.06	0.02	5.02	3.23
Morocco	6.13	16.76	237.54	0.03	6.48	0.02	6.00	96.08	0.66	0.03	5.00	0.68	0.02	5.00	79.59
Namibia	4.18	5.24	12.67	0.01	6.45	0.01	54.51	3.15	>10	0.01	5.99	>10	0.01	9.00	2.63
Nebraska	3.55	2.51	113.55	0.01	6.49	0.01	28.70	30.04	0.14	0.02	5.01	1.10	0.01	15.14	10.82
Nepal	0.00	7.32	51.49	0.00	6.29	0.01	8.60	41.18	0.09	0.02	60.00	0.07	0.01	18.26	13.53
New Hampshire	30.00	8.92	43.79	0.07	13.60	0.07	57.55	27.23	>10	0.07	17.00	>10	0.03	42.04	7.14
New Jersey	10.97	2.87	4895.44	0.08	8.60	0.08	58.97	644.88	0.21	0.08	8.72	0.25	0.02	23.14	82.54
New Mexico	4.95	4.12	231.03	0.03	6.00	0.04	42.30	63.74	0.67	0.03	5.00	0.09	0.02	16.13	39.64
New York	4.70	2.02	19 330.62	0.08	6.45	0.07	50.50	1732.21	>10	0.08	5.00	>10	0.01	11.29	377.77
Nigeria	3.83	4.41	309.09	0.02	6.50	0.02	39.70	54.57	8.66	0.02	5.00	8.73	0.00	7.62	56.67
North Macedonia	16.58	12.83	119.33	0.05	6.47	0.03	6.00	56.56	0.72	0.05	5.00	0.23	0.03	9.18	17.10
Norway	3.02	0.00	129.09	0.03	13.30	0.03	59.01	19.39	>10	0.03	12.91	9.89	0.02	59.87	5.92
Ohio	30.00	9.77	687.98	0.07	7.50	0.04	38.90	613.82	0.09	0.07	5.00	0.06	0.02	5.02	49.01
Oman	4.10	6.35	125.72	0.01	14.70	0.01	43.80	39.11	0.03	0.01	52.13	>10	0.01	20.01	5.35
Panama	7.89	8.43	192.07	0.02	5.99	0.02	28.00	47.92	9.77	0.02	5.00	0.56	0.02	15.23	38.57

TABLE III. (*Continued.*)

Country	$\beta_F^{I,opt}$ (10^{-4} d^{-1})	$\beta_F^{II,opt}$ (10^{-4} d^{-1})	$\langle \mathscr{E}_{KIN2} \rangle$ (—)	$f_{F,DEL}^{I,opt}$ (—)	$T_{F,DEL}^{I,opt}$ (d)	$f_{F,DEL}^{II,opt}$ (—)	$T_{F,DEL}^{II,opt}$ (d)	$\langle \mathscr{E}_{DEL2} \rangle$ (—)	$s_{HER}^{I,opt}$ (d^{-1})	$f_{F,HER}^{I,opt}$ (—)	$T_{F,HER}^{I,opt}$ (d)	$s_{HER}^{II,opt}$ (d^{-1})	$f_{F,HER}^{II,opt}$ (—)	$T_{F,HER}^{II,opt}$ (d)	$\langle \mathscr{E}_{HER2} \rangle$ (—)
Pakistan	9.24	13.38	634.27	0.02	6.00	0.02	11.70	91.63	1.03	0.02	5.00	0.06	0.07	59.70	78.06
Paraguay	10.68	6.37	80.61	0.02	7.20	0.03	50.90	34.63	>10	0.02	6.00	0.32	0.02	8.33	14.61
Pennsylvania	24.66	8.34	293.55	0.08	12.00	0.06	48.60	822.34	>10	0.08	10.67	>10	0.02	16.96	75.92
Peru	29.26	12.18	4171.68	0.07	6.01	0.04	5.99	2429.67	0.05	0.08	5.00	1.00	0.02	5.00	320.60
Poland	13.02	12.64	502.35	0.05	6.50	0.02	11.60	466.93	0.93	0.04	5.00	0.10	0.02	14.44	76.52
Portugal	7.76	8.53	381.36	0.04	6.60	0.04	40.80	235.03	0.15	0.04	6.18	0.23	0.02	14.55	30.32
Qatar	0.59	0.00	61.92	0.00	30.30	0.00	30.40	5.05	0.12	0.00	23.35	0.01	0.00	22.87	1.83
Rhode Island	8.37	1.61	219.94	0.06	7.70	0.06	56.55	63.00	>10	0.06	9.00	0.13	0.02	27.25	9.86
Romania	30.00	14.75	238.61	0.07	6.50	0.08	59.00	578.73	0.02	0.17	60.00	0.05	0.03	8.34	64.98
Russia	6.76	9.55	1030.70	0.02	18.30	0.02	6.00	286.55	0.08	0.02	14.46	0.12	0.02	13.04	65.03
Senegal	5.63	30.00	56.75	0.02	9.20	0.02	51.80	8.07	1.50	0.02	8.99	2.18	0.04	12.24	6.30
Somalia	0.00	0.00	80.48	0.03	6.48	0.03	52.58	5.60	>10	0.03	6.00	0.09	0.03	51.18	5.50
South Africa	14.84	21.89	359.86	0.02	12.50	0.03	6.00	427.41	0.06	0.03	12.98	0.33	0.04	8.95	136.62
South Dakota	0.00	9.01	85.72	0.01	14.30	0.02	21.70	11.94	>10	0.02	15.95	>10	0.02	21.39	12.02
State of Palestine	4.23	8.44	18.49	0.01	6.50	0.01	7.10	9.47	0.33	0.01	15.17	0.16	0.01	14.53	4.07
Sudan	3.42	3.96	687.79	0.09	6.49	0.09	56.50	43.86	1.11	0.08	5.00	2.10	0.03	5.06	25.44
Suriname	10.72	0.00	23.50	0.02	10.30	0.02	33.90	1.81	0.21	0.02	9.75	0.17	0.26	34.05	1.74
Switzerland	30.00	7.98	270.56	0.06	9.00	0.06	57.60	277.62	0.00	0.12	44.01	0.12	0.02	23.28	89.35
Tennessee	5.77	12.92	306.75	0.01	6.00	0.01	9.70	80.18	0.03	0.02	14.68	0.07	0.01	5.01	59.32
Texas	8.56	6.49	560.22	0.02	14.70	0.02	34.70	328.95	0.16	0.02	12.70	0.15	0.01	5.00	231.79
Turkey	14.65	11.35	590.40	0.01	6.00	0.01	6.50	336.94	7.84	0.01	5.00	0.02	0.02	60.00	157.94
United Arab Emirates	1.51	1.46	143.25	0.01	6.50	0.01	59.00	41.36	8.23	0.01	5.00	8.60	0.00	15.79	17.80
Utah	3.24	1.89	62.25	0.01	5.99	0.01	55.50	23.63	0.06	0.01	5.01	>10	0.01	24.01	13.52
Uzbekistan	6.38	9.15	49.11	0.01	14.30	0.01	5.99	9.00	5.93	0.01	13.87	0.90	0.01	5.01	7.23
Virginia	4.13	1.19	932.89	0.03	6.49	0.03	38.00	308.87	0.08	0.04	5.00	7.20	0.02	28.88	71.46
Wisconsin	18.53	7.89	105.98	0.04	6.50	0.03	59.01	225.11	6.38	0.03	5.00	0.23	0.01	19.10	49.77
Zambia	5.02	8.06	152.56	0.02	6.44	0.02	34.40	18.70	0.86	0.02	5.00	1.45	0.03	28.34	20.39
Zimbabwe	6.49	9.30	69.50	0.03	8.46	0.03	11.42	5.26	1.06	0.03	7.71	0.13	0.03	5.21	5.01

TABLE IV. Model-specific time-averaged absolute and normalized error measures according to Eq. (19) and Eq. (28).

Country	$\langle \mathscr{E}_{\mathrm{KIN}} \rangle$ (—)	$\langle \mathscr{E}_{\mathrm{DEL}} \rangle$ (—)	$\langle \mathscr{E}_{\mathrm{HER}} \rangle$ (—)	$\langle \mathscr{E}_{\mathrm{KIN2}} \rangle$ (—)	$\langle \mathscr{E}_{\mathrm{DEL2}} \rangle$ (—)	$\langle \mathscr{E}_{\mathrm{HER2}} \rangle$ (—)	$F_{\max}$ (—)	$\langle \mathscr{R}_{\mathrm{KIN}} \rangle$ (—)	$\langle \mathscr{R}_{\mathrm{DEL}} \rangle$ (—)	$\langle \mathscr{R}_{\mathrm{HER}} \rangle$ (—)	$\langle \mathscr{R}_{\mathrm{KIN2}} \rangle$ (—)	$\langle \mathscr{R}_{\mathrm{DEL2}} \rangle$ (—)	$\langle \mathscr{R}_{\mathrm{HER2}} \rangle$ (—)
Afghanistan	162.51	60.53	46.69	169.79	44.34	18.03	2201	0.0738	0.0275	0.0212	0.0771	0.0201	0.0082
Albania	115.54	33.17	32.70	121.44	31.14	15.19	1181	0.0978	0.0281	0.0277	0.1028	0.0264	0.0129
Andorra	50.79	24.33	23.75	15.95	18.78	1.53	84	0.6047	0.2896	0.2828	0.1899	0.2236	0.0182
Arizona	2143.82	338.52	337.77	1555.91	165.95	117.13	8864	0.2419	0.0382	0.0381	0.1755	0.0187	0.0132
Arkansas	62.08	44.64	35.50	120.54	31.64	31.76	3570	0.0174	0.0125	0.0099	0.0338	0.0089	0.0089
Armenia	67.57	53.65	42.45	40.27	31.71	5.60	2823	0.0239	0.0190	0.0150	0.0143	0.0112	0.0020
Australia	107.42	47.30	47.09	85.24	32.61	6.98	909	0.1182	0.0520	0.0518	0.0938	0.0359	0.0077
Austria	253.65	227.92	162.17	160.33	163.49	54.53	6222	0.0408	0.0366	0.0261	0.0258	0.0263	0.0088
Azerbaijan	95.70	31.56	21.25	44.02	26.26	6.74	2641	0.0362	0.0119	0.0080	0.0167	0.0099	0.0026
Bahrain	26.04	3.94	3.88	25.04	3.75	3.64	352	0.0740	0.0112	0.0110	0.0711	0.0106	0.0103
Bangladesh	600.08	77.08	64.60	610.18	62.76	60.00	7559	0.0794	0.0102	0.0085	0.0807	0.0083	0.0079
Belarus	110.76	66.79	25.03	187.86	46.49	9.23	1424	0.0778	0.0469	0.0176	0.1319	0.0326	0.0065
Belgium	7389.85	3676.68	3526.52	5976.70	2067.41	217.02	194 41	0.3801	0.1891	0.1814	0.3074	0.1063	0.0112
Bolivia	1004.58	55.73	43.98	829.27	49.94	33.94	9149	0.1098	0.0061	0.0048	0.0906	0.0055	0.0037
Bosnia and Herzegovina	51.74	45.88	45.34	92.16	39.29	25.15	4050	0.0128	0.0113	0.0112	0.0228	0.0097	0.0062
Brazil	27 244.64	10 622.69	10 476.22	19 821.18	8218.72	7396.08	194 976	0.1397	0.0545	0.0537	0.1017	0.0422	0.0379
Bulgaria	61.52	58.65	38.06	42.20	50.09	26.69	7576	0.0081	0.0077	0.0050	0.0056	0.0066	0.0035
California	5265.39	1518.19	1512.63	2682.75	763.62	975.79	26 343	0.1999	0.0576	0.0574	0.1018	0.0290	0.0370
Canada	3233.87	1807.43	1782.96	855.03	690.36	74.84	15 606	0.2072	0.1158	0.1142	0.0548	0.0442	0.0048
Chile	1395.10	72.88	67.32	1789.07	67.90	60.62	16 608	0.0840	0.0044	0.0041	0.1077	0.0041	0.0037
China	1263.72	251.68	135.14	1384.12	135.60	94.78	4634	0.2727	0.0543	0.0292	0.2987	0.0293	0.0205
Colorado	1138.63	468.02	468.02	598.74	268.34	26.66	4814	0.2365	0.0972	0.0972	0.1244	0.0557	0.0055
Connecticut	2921.95	836.92	826.60	1948.87	187.05	53.68	5995	0.4874	0.1396	0.1379	0.3251	0.0312	0.0090
Costa Rica	73.87	14.87	11.86	78.17	14.85	11.00	2185	0.0338	0.0068	0.0054	0.0358	0.0068	0.0050
Cote d'Ivoire	80.44	6.66	6.48	37.77	6.49	6.39	137	0.5872	0.0486	0.0473	0.2757	0.0474	0.0466
Croatia	115.15	32.41	28.93	95.93	26.30	15.47	3920	0.0294	0.0083	0.0074	0.0245	0.0067	0.0039
Czechia	330.37	125.18	108.53	331.05	110.06	79.22	11 813	0.0280	0.0106	0.0092	0.0280	0.0093	0.0067
Delaware	403.38	109.12	107.75	169.97	78.81	10.14	926	0.4356	0.1178	0.1164	0.1836	0.0851	0.0109
Dem. Rep. Congo	90.86	16.45	16.09	87.08	14.36	13.53	591	0.1537	0.0278	0.0272	0.1473	0.0243	0.0229
Denmark	433.59	214.49	211.65	56.64	105.80	17.34	1298	0.3340	0.1652	0.1631	0.0436	0.0815	0.0134
Dominican Republic	714.78	145.00	143.42	413.56	105.34	92.86	2414	0.2961	0.0601	0.0594	0.1713	0.0436	0.0385
Ecuador	3118.53	1569.36	1556.14	3029.74	1490.89	119.80	14 034	0.2222	0.1118	0.1109	0.2159	0.1062	0.0085
Egypt	584.30	131.77	61.63	844.86	80.44	56.64	7631	0.0766	0.0173	0.0081	0.1107	0.0105	0.0074
El Salvador	102.44	10.88	10.09	158.50	17.42	9.94	1336	0.0767	0.0081	0.0076	0.1186	0.0130	0.0074
Estonia	27.16	11.72	11.62	51.43	4.70	3.59	229	0.1186	0.0512	0.0508	0.2246	0.0205	0.0157
Eswatini	17.93	2.74	2.70	20.11	3.24	2.21	205	0.0875	0.0134	0.0132	0.0981	0.0158	0.0108
Finland	233.24	71.99	71.78	78.92	27.07	7.53	561	0.4158	0.1283	0.1280	0.1407	0.0483	0.0134
France	21 315.15	14 766.54	14 682.89	17 462.61	9908.80	592.16	64 780	0.3290	0.2279	0.2267	0.2696	0.1530	0.0091
Germany	4094.74	1408.29	1376.55	887.36	614.16	290.67	34 194	0.1198	0.0412	0.0403	0.0260	0.0180	0.0085

TABLE IV. (*Continued.*)

Country	$\langle \mathscr{E}_{\mathrm{KIN}} \rangle$ (—)	$\langle \mathscr{E}_{\mathrm{DEL}} \rangle$ (—)	$\langle \mathscr{E}_{\mathrm{HER}} \rangle$ (—)	$\langle \mathscr{E}_{\mathrm{KIN2}} \rangle$ (—)	$\langle \mathscr{E}_{\mathrm{DEL2}} \rangle$ (—)	$\langle \mathscr{E}_{\mathrm{HER2}} \rangle$ (—)	$F_{\max}$ (—)	$\langle \mathscr{R}_{\mathrm{KIN}} \rangle$ (—)	$\langle \mathscr{R}_{\mathrm{DEL}} \rangle$ (—)	$\langle \mathscr{R}_{\mathrm{HER}} \rangle$ (—)	$\langle \mathscr{R}_{\mathrm{KIN2}} \rangle$ (—)	$\langle \mathscr{R}_{\mathrm{DEL2}} \rangle$ (—)	$\langle \mathscr{R}_{\mathrm{HER2}} \rangle$ (—)
Ghana	179.90	7.63	6.45	179.91	6.34	4.71	335	0.5370	0.0228	0.0193	0.5370	0.0189	0.0141
Greece	150.02	70.25	69.75	145.40	60.06	52.77	4838	0.0310	0.0145	0.0144	0.0301	0.0124	0.0109
Haiti	142.51	8.32	5.90	69.26	7.78	4.96	236	0.6038	0.0353	0.0250	0.2935	0.0330	0.0210
Hawaii	54.24	7.31	5.68	50.14	6.91	2.71	288	0.1883	0.0254	0.0197	0.1741	0.0240	0.0094
Hungary	393.18	273.25	204.67	213.06	184.77	47.99	9537	0.0412	0.0287	0.0215	0.0223	0.0194	0.0050
Indonesia	843.63	996.76	988.69	748.48	679.91	636.37	22 138	0.0381	0.0450	0.0447	0.0338	0.0307	0.0287
Ireland	1396.31	446.55	443.74	474.73	183.69	14.93	2237	0.6242	0.1996	0.1984	0.2122	0.0821	0.0067
Israel	120.02	79.81	59.75	118.23	67.22	12.05	3325	0.0361	0.0240	0.0180	0.0356	0.0202	0.0036
Italy	23 343.57	7298.56	7298.84	12 006.31	1816.28	233.24	74 159	0.3148	0.0984	0.0984	0.1619	0.0245	0.0031
Kansas	445.87	64.06	59.58	431.26	49.18	39.42	2788	0.1599	0.0230	0.0214	0.1547	0.0176	0.0141
Kazakhstan	109.36	64.25	58.44	132.27	64.99	49.20	2286	0.0478	0.0281	0.0256	0.0579	0.0284	0.0215
Kenya	141.41	35.73	33.80	165.44	34.86	21.95	1670	0.0847	0.0214	0.0202	0.0991	0.0209	0.0131
Kosovo	163.86	59.02	50.89	16.03	37.08	10.33	1336	0.1227	0.0442	0.0381	0.0120	0.0278	0.0077
Malawi	106.38	4.47	4.48	106.38	4.06	4.18	189	0.5628	0.0236	0.0237	0.5628	0.0215	0.0221
Malaysia	85.91	43.33	36.73	53.05	29.60	9.55	471	0.1824	0.0920	0.0780	0.1126	0.0629	0.0203
Massachusetts	3860.40	1070.64	1065.22	1049.05	283.80	201.13	12 423	0.3107	0.0862	0.0857	0.0844	0.0228	0.0162
Mauritania	33.54	14.33	13.99	74.44	13.76	12.55	347	0.0967	0.0413	0.0403	0.2145	0.0397	0.0362
Mexico	25 788.29	3956.11	3272.22	25 788.21	2062.82	943.14	124 897	0.2065	0.0317	0.0262	0.2065	0.0165	0.0076
Michigan	4601.48	1761.48	1755.66	841.48	854.56	72.86	13 018	0.3535	0.1353	0.1349	0.0646	0.0656	0.0056
Minnesota	819.50	432.21	430.26	601.83	293.12	38.29	5463	0.1500	0.0791	0.0788	0.1102	0.0537	0.0070
Montenegro	50.51	12.80	12.32	50.37	11.74	3.23	682	0.0741	0.0188	0.0181	0.0738	0.0172	0.0047
Morocco	171.88	104.91	98.66	237.54	96.08	79.59	7388	0.0233	0.0142	0.0134	0.0322	0.0130	0.0108
Namibia	13.35	3.39	3.21	12.67	3.15	2.63	205	0.0651	0.0166	0.0157	0.0618	0.0154	0.0128
Nebraska	143.59	43.91	41.88	113.55	30.04	10.82	1651	0.0870	0.0266	0.0254	0.0688	0.0182	0.0066
Nepal	101.66	47.69	29.68	51.49	41.18	13.53	2703	0.0376	0.0176	0.0110	0.0190	0.0152	0.0050
New Hampshire	206.44	68.12	68.19	43.79	27.23	7.14	759	0.2720	0.0898	0.0898	0.0577	0.0359	0.0094
New Jersey	9089.18	2277.78	2251.66	4895.44	644.88	82.54	19 184	0.4738	0.1187	0.1174	0.2552	0.0336	0.0043
New Mexico	268.90	125.46	124.76	231.03	63.74	39.64	2477	0.1086	0.0507	0.0504	0.0933	0.0257	0.0160
New York	22 331.89	4467.88	4474.14	19 330.62	1732.21	377.77	38 007	0.5876	0.1176	0.1177	0.5086	0.0456	0.0099
Nigeria	302.88	78.11	77.03	309.09	54.57	56.67	1289	0.2350	0.0606	0.0598	0.2398	0.0423	0.0440
North Macedonia	180.69	93.27	73.19	119.33	56.56	17.10	2503	0.0722	0.0373	0.0292	0.0477	0.0226	0.0068
Norway	174.39	56.34	56.11	129.09	19.39	5.92	436	0.4000	0.1292	0.1287	0.2961	0.0445	0.0136
Ohio	1714.77	823.38	811.88	687.98	613.82	49.01	13 237	0.1295	0.0622	0.0613	0.0520	0.0464	0.0037
Oman	151.06	53.46	10.94	125.72	39.11	5.35	1499	0.1008	0.0357	0.0073	0.0839	0.0261	0.0036
Panama	181.41	126.81	125.95	192.07	47.92	38.57	4022	0.0451	0.0315	0.0313	0.0478	0.0119	0.0096
Pakistan	239.55	174.43	169.05	634.27	91.63	78.06	10 105	0.0237	0.0173	0.0167	0.0628	0.0091	0.0077
Paraguay	188.68	25.58	25.30	80.61	34.63	14.61	2262	0.0834	0.0113	0.0112	0.0356	0.0153	0.0065
Pennsylvania	2857.13	1461.34	1461.39	293.55	822.34	75.92	16 073	0.1778	0.0909	0.0909	0.0183	0.0512	0.0047
Peru	7639.74	3173.60	3127.06	4171.68	2429.67	320.60	37 680	0.2028	0.0842	0.0830	0.1107	0.0645	0.0085

TABLE IV. (*Continued.*)

Country	$\langle \mathscr{E}_{\mathrm{KIN}} \rangle$ (—)	$\langle \mathscr{E}_{\mathrm{DEL}} \rangle$ (—)	$\langle \mathscr{E}_{\mathrm{HER}} \rangle$ (—)	$\langle \mathscr{E}_{\mathrm{KIN2}} \rangle$ (—)	$\langle \mathscr{E}_{\mathrm{DEL2}} \rangle$ (—)	$\langle \mathscr{E}_{\mathrm{HER2}} \rangle$ (—)	$F_{\max}$ (—)	$\langle \mathscr{R}_{\mathrm{KIN}} \rangle$ (—)	$\langle \mathscr{R}_{\mathrm{DEL}} \rangle$ (—)	$\langle \mathscr{R}_{\mathrm{HER}} \rangle$ (—)	$\langle \mathscr{R}_{\mathrm{KIN2}} \rangle$ (—)	$\langle \mathscr{R}_{\mathrm{DEL2}} \rangle$ (—)	$\langle \mathscr{R}_{\mathrm{HER2}} \rangle$ (—)
Poland	499.77	605.27	380.11	502.35	466.93	76.52	28 556	0.0175	0.0212	0.0133	0.0176	0.0164	0.0027
Portugal	397.55	352.23	315.79	381.36	235.03	30.32	6906	0.0576	0.0510	0.0457	0.0552	0.0340	0.0044
Qatar	62.53	5.51	2.32	61.92	5.05	1.83	245	0.2552	0.0225	0.0095	0.2527	0.0206	0.0075
Rhode Island	605.04	189.67	189.27	219.94	63.00	9.86	1911	0.3166	0.0992	0.0990	0.1151	0.0330	0.0052
Romania	600.12	850.67	764.87	238.61	578.73	64.98	15 767	0.0381	0.0540	0.0485	0.0151	0.0367	0.0041
Russia	2638.08	664.97	663.64	1030.70	286.55	65.03	57 019	0.0463	0.0117	0.0116	0.0181	0.0050	0.0011
Senegal	53.34	7.19	7.17	56.75	8.07	6.30	410	0.1301	0.0175	0.0175	0.1384	0.0197	0.0154
Somalia	80.48	8.73	8.62	80.48	5.60	5.50	130	0.6191	0.0671	0.0663	0.6191	0.0430	0.0423
South Africa	498.81	775.22	231.02	359.86	427.41	136.62	28 921	0.0172	0.0268	0.0080	0.0124	0.0148	0.0047
South Dakota	31.70	12.84	12.85	85.72	11.94	12.02	1488	0.0213	0.0086	0.0086	0.0576	0.0080	0.0081
State of Palestine	83.06	17.32	16.79	18.49	9.47	4.07	1400	0.0593	0.0124	0.0120	0.0132	0.0068	0.0029
Sudan	676.19	60.03	59.97	687.79	43.86	25.44	1468	0.4606	0.0409	0.0409	0.4685	0.0299	0.0173
Suriname	24.03	1.82	1.78	23.50	1.81	1.74	122	0.1970	0.0149	0.0146	0.1926	0.0148	0.0143
Switzerland	1008.01	548.10	469.10	270.56	277.62	89.35	7645	0.1319	0.0717	0.0614	0.0354	0.0363	0.0117
Tennessee	265.40	98.78	61.07	306.75	80.18	59.32	6907	0.0384	0.0143	0.0088	0.0444	0.0116	0.0086
Texas	1325.58	578.44	578.32	560.22	328.95	231.79	28 227	0.0470	0.0205	0.0205	0.0198	0.0117	0.0082
Turkey	488.97	373.10	355.55	590.40	336.94	157.94	20 881	0.0234	0.0179	0.0170	0.0283	0.0161	0.0076
United Arab Emirates	141.56	75.71	75.43	143.25	41.36	17.80	669	0.2116	0.1132	0.1128	0.2141	0.0618	0.0266
Utah	122.11	61.54	61.33	62.25	23.63	13.52	1269	0.0962	0.0485	0.0483	0.0491	0.0186	0.0107
Uzbekistan	58.92	12.51	12.19	49.11	9.00	7.23	614	0.0960	0.0204	0.0199	0.0800	0.0147	0.0118
Virginia	1353.94	377.81	377.83	932.89	308.87	71.46	5032	0.2691	0.0751	0.0751	0.1854	0.0614	0.0142
Wisconsin	235.32	268.78	253.41	105.98	225.11	49.77	4859	0.0484	0.0553	0.0522	0.0218	0.0463	0.0102
Zambia	140.03	22.41	22.04	152.56	18.70	20.39	388	0.3609	0.0578	0.0568	0.3932	0.0482	0.0526
Zimbabwe	70.91	5.51	5.45	69.50	5.26	5.01	363	0.1954	0.0152	0.0150	0.1915	0.0145	0.0138

TABLE V. Model-specific coefficients of determination according to Eq. (27).

Country	R^2_{KIN} (—)	R^2_{DEL} (—)	R^2_{HER} (—)	R^2_{KIN2} (—)	R^2_{DEL2} (—)	R^2_{HER2} (—)
Afghanistan	0.9191	0.9787	0.9846	0.9128	0.9909	0.9986
Albania	0.7991	0.9678	0.9740	0.7839	0.9683	0.9956
Andorra	−5.6649	−3.1722	−2.9544	0.1408	−2.6712	0.9869
Arizona	0.1019	0.9599	0.9634	0.5432	0.9921	0.9944
Arkansas	0.9925	0.9969	0.9980	0.9734	0.9984	0.9983
Armenia	0.9886	0.9925	0.9939	0.9946	0.9959	0.9999
Australia	0.8701	0.9674	0.9676	0.8883	0.9778	0.9992
Austria	0.9456	0.9617	0.9769	0.9513	0.9731	0.9955
Azerbaijan	0.9570	0.9773	0.9975	0.9852	0.9863	0.9995
Bahrain	0.9289	0.9985	0.9986	0.9410	0.9986	0.9986
Bangladesh	0.9250	0.9980	0.9989	0.9250	0.9989	0.9989
Belarus	0.8739	0.9630	0.9914	0.6525	0.9734	0.9991
Belgium	−1.6718	−0.9789	−0.7575	−0.7391	−0.4383	0.9953
Bolivia	0.8863	0.9996	0.9997	0.9230	0.9997	0.9998
Bosnia and Herzegovina	0.9965	0.9971	0.9974	0.9905	0.9977	0.9989
Brazil	0.7781	0.9577	0.9588	0.8814	0.9732	0.9735
Bulgaria	0.9980	0.9985	0.9990	0.9987	0.9987	0.9996
California	0.3479	0.9044	0.9166	0.8342	0.9768	0.9612
Canada	0.2828	0.6493	0.6208	0.9357	0.9210	0.9993
Chile	0.9177	0.9996	0.9996	0.8626	0.9996	0.9996
China	−0.3581	0.8493	0.9668	−0.6412	0.9517	0.9657
Colorado	−0.3366	0.6672	0.6648	0.6290	0.8521	0.9983
Connecticut	−2.9238	0.3884	0.4484	−0.7358	0.9629	0.9979
Costa Rica	0.9747	0.9991	0.9994	0.9729	0.9991	0.9995
Cote d'Ivoire	−2.6992	0.9642	0.9662	0.2541	0.9669	0.9674
Croatia	0.9591	0.9979	0.9984	0.9690	0.9983	0.9990
Czechia	0.9723	0.9977	0.9984	0.9729	0.9979	0.9984
Delaware	−1.9764	0.6974	0.7355	0.4522	0.7779	0.9967
Dem. Rep. Congo	0.2871	0.9340	0.9356	0.3730	0.9491	0.9732
Denmark	−2.1232	−0.1720	−0.1375	0.9350	0.6172	0.9881
Dominican Republic	0.1084	0.9551	0.9558	0.7308	0.9779	0.9795
Ecuador	0.4651	0.8395	0.8415	0.4873	0.8453	0.9982
Egypt	0.9283	0.9957	0.9990	0.8640	0.9982	0.9991
El Salvador	0.9134	0.9989	0.9991	0.8093	0.9935	0.9991
Estonia	0.5106	0.8217	0.8202	−0.7391	0.9699	0.9836
Eswatini	0.7921	0.9936	0.9940	0.7537	0.9829	0.9964
Finland	−2.2283	0.3989	0.3913	0.5456	0.9031	0.9922
France	−1.1195	−0.2893	−0.2848	−0.4202	0.0877	0.9973
Germany	0.5025	0.8912	0.8962	0.9674	0.9820	0.9948
Ghana	−1.9060	0.9940	0.9956	−1.9062	0.9949	0.9971
Greece	0.9509	0.9935	0.9934	0.9514	0.9940	0.9923
Haiti	−2.3813	0.9843	0.9937	0.2589	0.9853	0.9952
Hawaii	0.4136	0.9916	0.9952	0.4351	0.9930	0.9980
Hungary	0.9613	0.9792	0.9864	0.9869	0.9857	0.9990
Indonesia	0.9789	0.9659	0.9664	0.9838	0.9788	0.9841
Ireland	−4.2866	−0.1687	−0.1652	0.3819	0.5837	0.9988
Israel	0.9775	0.9920	0.9944	0.9757	0.9931	0.9998
Italy	−1.2471	0.4979	0.4947	0.4150	0.9295	0.9996

TABLE V. (*Continued.*)

Country	R^2_{KIN} (—)	R^2_{DEL} (—)	R^2_{HER} (—)	R^2_{KIN2} (—)	R^2_{DEL2} (—)	R^2_{HER2} (—)
Kansas	0.0836	0.9853	0.9876	0.0063	0.9913	0.9935
Kazakhstan	0.9718	0.9903	0.9901	0.9624	0.9895	0.9921
Kenya	0.8904	0.9934	0.9941	0.8552	0.9933	0.9973
Kosovo	0.7110	0.9022	0.9547	0.9977	0.9657	0.9988
Malawi	−1.6772	0.9934	0.9935	−1.6773	0.9934	0.9933
Malaysia	0.3015	0.6813	0.8056	0.6804	0.7543	0.9814
Massachusetts	−0.4859	0.7348	0.7711	0.8776	0.9827	0.9937
Mauritania	0.7131	0.9285	0.9324	−0.0961	0.9248	0.9359
Mexico	0.4127	0.9831	0.9865	0.4127	0.9952	0.9989
Michigan	−1.8219	0.3489	0.3645	0.8966	0.8063	0.9987
Minnesota	0.5305	0.8083	0.8118	0.7477	0.8916	0.9973
Montenegro	0.8609	0.9924	0.9931	0.8634	0.9927	0.9993
Morocco	0.9890	0.9965	0.9969	0.9797	0.9967	0.9981
Namibia	0.9128	0.9936	0.9946	0.9227	0.9935	0.9965
Nebraska	0.8277	0.9798	0.9836	0.8786	0.9872	0.9987
Nepal	0.9735	0.9934	0.9972	0.9851	0.9942	0.9994
New Hampshire	−0.4577	0.7806	0.7778	0.9256	0.9321	0.9977
New Jersey	−2.2400	0.4818	0.6009	0.0776	0.9667	0.9995
New Mexico	0.7457	0.9001	0.9103	0.8113	0.9808	0.9887
New York	−4.7500	0.4773	0.4794	−3.2930	0.9451	0.9941
Nigeria	0.4475	0.9513	0.9525	0.4237	0.9718	0.9705
North Macedonia	0.8884	0.9695	0.9765	0.9492	0.9817	0.9987
Norway	−2.3801	0.3435	0.3327	−0.9966	0.9259	0.9933
Ohio	0.6335	0.8827	0.8913	0.9349	0.9226	0.9994
Oman	0.8216	0.9713	0.9989	0.8830	0.9834	0.9998
Panama	0.9598	0.9762	0.9757	0.9548	0.9976	0.9982
Pakistan	0.9882	0.9949	0.9954	0.9474	0.9982	0.9985
Paraguay	0.8434	0.9978	0.9979	0.9747	0.9902	0.9992
Pennsylvania	0.2677	0.7266	0.7247	0.9908	0.8847	0.9990
Peru	0.5930	0.9042	0.9066	0.8828	0.9250	0.9982
Poland	0.9860	0.9909	0.9948	0.9856	0.9926	0.9998
Portugal	0.8984	0.8922	0.9266	0.9110	0.9412	0.9994
Qatar	0.2893	0.9919	0.9990	0.2935	0.9935	0.9992
Rhode Island	−0.9539	0.6499	0.6721	0.7188	0.9506	0.9991
Romania	0.9737	0.9436	0.9499	0.9953	0.9540	0.9996
Russia	0.9492	0.9961	0.9961	0.9883	0.9991	1.0000
Senegal	0.7756	0.9941	0.9941	0.7506	0.9914	0.9948
Somalia	−4.6607	0.8979	0.9018	−4.6609	0.9407	0.9345
South Africa	0.9950	0.9845	0.9981	0.9971	0.9958	0.9995
South Dakota	0.9710	0.9976	0.9977	0.9166	0.9977	0.9981
State of Palestine	0.8847	0.9929	0.9922	0.9926	0.9966	0.9996
Sudan	−1.6530	0.9511	0.9500	−1.7482	0.9797	0.9957
Suriname	0.5469	0.9971	0.9972	0.5653	0.9971	0.9973
Switzerland	0.5459	0.7286	0.8194	0.9647	0.8658	0.9921
Tennessee	0.9514	0.9947	0.9980	0.9582	0.9964	0.9981
Texas	0.9655	0.9886	0.9887	0.9945	0.9974	0.9983
Turkey	0.9801	0.9904	0.9916	0.9599	0.9903	0.9979
United Arab Emirates	0.3365	0.7903	0.7911	0.3179	0.9013	0.9729

TABLE V. (*Continued.*)

Country	R^2_{KIN} (—)	R^2_{DEL} (—)	R^2_{HER} (—)	R^2_{KIN2} (—)	R^2_{DEL2} (—)	R^2_{HER2} (—)
Utah	0.8245	0.9386	0.9377	0.9562	0.9839	0.9967
Uzbekistan	0.8977	0.9941	0.9950	0.9302	0.9972	0.9984
Virginia	−0.1140	0.8548	0.8530	0.4800	0.9208	0.9948
Wisconsin	0.9499	0.9326	0.9320	0.9864	0.9345	0.9972
Zambia	−0.3864	0.9566	0.9586	−0.6414	0.9654	0.9611
Zimbabwe	0.3476	0.9956	0.9958	0.3820	0.9964	0.9965

knowledge of the authors, this marks a new level of precision in the equation-based description of pandemic-related fatality trends.

Hence, our novel approach adds an original aspect to the few recent research endeavors which employ convolution integrals in the context of COVID-19 modeling, so as to relate, in quite different ways, the number of infected people over time to numbers or also to rates of newly infected people. In this context, three main paths were followed:

- Convolution integrals were employed to spatial variables in the context of social heterogeneity.[27]
- The number of previously infected persons was linked to the evolution of the newly infected people, with the corresponding kernels being Gaussian or Weibull probability density functions associated with the incubation period, which varies from patient to patient.[65]
- The number of previously infected people was linked to the rate of newly confirmed cases, with the corresponding kernels being normal distributions, delta-functions, or Weibull distributions,[66] and similar approaches have been applied to the number of susceptibles[25,26] with calling the respective kernel the "evolution of infectiousness" and "infectivity probability," respectively, and choosing a Gamma-distribution for the latter.

As a common characteristic, all these recent endeavors, which somehow mark the advent of hereditary epidemiology as well, rely upon a statistical interpretation of the kernels occurring in the integro-differential equations, with classical statistical choices such as Gaussian, Weibull, Gamma, or delta functions. As stated above, we here took a distinctively different perspective, by adopting a mechanical rather than statistical motivation for proposing integrodifferential equations relating infections to fatality trends, and we supported the novel formulation by comparison with very many, world-widely recorded data.

In this context, it is appropriate to make a few comments on the nature of the experimental (or rather observational) data against which we have tested the three modeling strategies studied in this paper: the confirmed cases typically relate to persons who have either felt symptoms of COVID-19, or have undergone polymerase chain reaction-testing (commonly known as PCR-testing) or antigen-testing. Symptomatic persons are, as a rule, already infectious,[67] and the share of asymptotically or presymptomically tested persons who are already infectious is typically very small.[68] Hence, within the precision limits of mathematical models based on compartmentalization of the population, it is safe to say that the confirmed cases recorded in publicly available data bases (such as Worldometer[58]) refer to infectious, rather than solely exposed persons. Hence, the choice of a benchmark model in the SEIR format, with the letter E standing for the population of exposed persons (while the letters S, I, R stand for the populations of susceptible, infectious, and recovered persons), is rather not advisable. In the same context, the question may arise whether variable I, occurring, for example, in Eq. (15), should represent "infectious" rather than "infected" persons. However, before full recovery (and hence, before leaving the compartment represented by the letter I), those persons are not infectious any more.[68] Thus, infected appears as an appropriate term for the compartment referred to by variable I.

It is also interesting to discuss different modifications, extensions, and further application ranges of our novel approach: currently, all model parameters are evaluated country-, US state-, or territory-specifically. This appears as a natural choice when considering that healthcare systems, the main drivers of fatality trends, are typically defined at this geographical level, and the wide agreement on this reasoning is reflected by the very existence of the comprehensive Worldometer database,[58] the data fundament of the present study. Still, also data associated with larger geographical entities, such as continents,[69,70] or smaller entities such as regions, provinces, countries, or districts,[25,28,29] could, in principle, enter the optimization process of Sec. III of the present paper. Regional data may be particularly interesting for countries with diverse settlement structures such as Sweden or Switzerland. At the same time, the partitioning of the global population hit by the pandemic need not necessarily be driven by geographical categories alone, with three additional factors being of eminent interest in the context of COVID-19 fatality trends: age, immune level, and virus mutations.[71–77] Accordingly, a geography-specific population may be further subdivided into different groups discriminated by age (e.g., resolved into decades), immune level (e.g., not-infected–not-vaccinated, partially vaccinated, fully vaccinated, recovered), or virus clade (e.g., wildtype, alpha variant, delta variant). Correspondingly optimized model parameters may provide valuable quantitative insight into the dynamics of mortality in these groups, and hence in the effectiveness of different strategies, such as reducing the contacts of the elderly, or vaccination. Still, we have to be aware that age-, vaccination-, and mutation-specific data are only sporadically available at the level of countries,[78] so that—for the time being—the subdivision of all 102 population sets investigated here into several age and/or immune level groups is simply impossible.

It is advisable to link our novel modeling approach to the standardly used epidemiological terminology, so as to highlight similarities as well as differences of the epidemiological model expressed by Eq. (4) with respect to earlier investigations, such as the work of

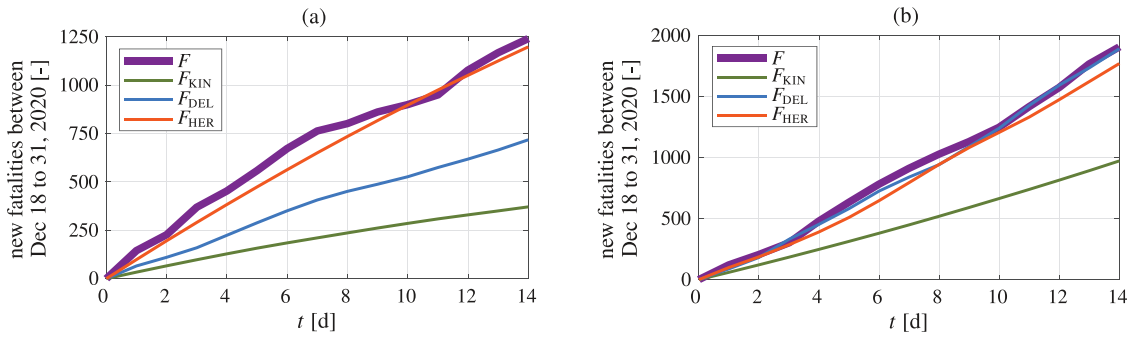

FIG. 4. Fatalities forecasts for a time period of two weeks, starting on December 18, 2021, based on the hereditary model (F_{HER}), the delay model (F_{DEL}), and the kinetics model (F_{KIN}); for (a) Austria ($R^2_{\mathrm{KIN}} = -1.8986$; $R^2_{\mathrm{DEL}} = -0.1268$; $R^2_{\mathrm{HER}} = 0.9618$), and (b) New York ($R^2_{\mathrm{KIN}} = 0.0463$; $R^2_{\mathrm{DEL}} = 0.9941$; $R^2_{\mathrm{HER}} = 0.9710$); the coefficients of determination relate to the recorded fatalities F.

Kaniadakis *et al.*[79] There, the logistic function was shown to very satisfactorily fit the overall evolution of the fatalities, referred to as $F(t)$ in the present paper, and denoted as "cumulative distribution function" by Kaniadakis *et al.*[79] We note that such an approach does not establish any link between infected and dead persons, as it was our goal when establishing Eq. (4). Still, the aforementioned good experience with the logistic function corroborated our choice of a logistic function for defining the fatality function J_{F} occurring in Eq. (4). However, the conceptual idea of Eq. (4) goes beyond the particular choice of J_{F} and is open toward any other mathematical formal appearing as appropriate for the representation of actual epidemic data. In this context, generalized logistic functions[80] may play a beneficial role in potential future applications.

An obvious practical application of our model concerns the forecast of future fatalities based on currently available datasets. In a corresponding preliminary study, we have calibrated the three models (HER, KIN, DEL) for two infection waves, but considered the time domain to end two weeks earlier than for the numerical studies presented above, that is, on December 17, 2020. The parameters of this time domain were optimized again via the fmincon-function of MATLAB, by minimizing the temporal average of the absolute errors between model-predicted fatality increments and recorded fatality increments, according to

$$\langle \mathscr{E}_m \rangle = \frac{1}{N_i} \sum_{i=1}^{N_i} |\Delta F_m(t_i) - \Delta F(t_i)|, \tag{29}$$

with $m = \mathrm{HER2}, \mathrm{DEL2}, \mathrm{KIN2}$, and with $\Delta F_m(t_i)$ and $\Delta F(t_i)$ standing for the model-predicted and recorded fatality increments, respectively. Thereafter, we have used the correspondingly optimized model parameters in order to forecast the fatalities for the time period from December 18 to 31, 2020. The quality of such forecasts was assessed by the coefficient of determination, R^2, between the forecast fatalities, and those actually encountered (see Fig. 4). For both Austria and New York, our novel hereditary approach performed very well, as indicated by an $R^2 > 0.95$, while the traditional kinetics model is associated with very low R^2-values. The delay model provided a good forecast in the case of New York, but performed badly in the case of Austria. This again underlines the validity of our novel approach.

Finally, we want to emphasize that the concept of hereditary epidemiology as proposed in this paper is applicable to many different phenomena taking place within the subpopulations already struck by an epidemic (in contrast to the transmission process between infected and susceptible individuals). In this sense, further application ranges for models similar to Eq. (4) may concern the transition from exposed to infectious persons, from infectious to hospitalized persons, or from hospitalized persons to patients requiring intensive care.

SUPPLEMENTARY MATERIAL

See the supplementary material for the raw data related to the each of the investigated countries, territories, and US states are provided. Furthermore, the optimized parameters obtained for each country are provided as well as graphical illustrations of the resulting fatality trends.

AUTHOR DECLARATIONS

Conflict of Interest

All authors declare that they have no conflict of interest.

DATA AVAILABILITY

The data that support the findings of this study are available within the article and its supplementary material.

ACKNOWLEDGMENTS

The authors gratefully acknowledge the financial support provided by the TU Wien Bibliothek through its Open Access Funding Programme.

REFERENCES

[1] H. Swapnarekha, H. S. Behera, J. Nayak, and B. Naik, "Role of intelligent computing in COVID-19 prognosis: A state-of-the-art review," Chaos, Solitons Fractals **138**, 109947 (2020).
[2] Y.-C. Chen, P.-E. Lu, and C.-S. Chang, "A time-dependent SIR model for COVID-19 with undetectable infected persons," IEEE Trans. Network Sci. Eng. **7**(4), 3279–3294 (2020).
[3] W. C. Roda, M. B. Varughese, D. Han, and M. Y. Li, "Why is it difficult to accurately predict the COVID-19 epidemic?," Infect. Dis. Modell. **5**, 271 (2020).
[4] M. Al-Raeei, "The forecasting of COVID-19 with mortality using SIRD epidemic model for the United States, Russia, China, and the Syrian Arab Republic," AIP Adv. **10**(6), 065325 (2020).

[5]A. Neves and G. Guerrero, "Predicting the evolution of the COVID-19 epidemic with the A-SIR model: Lombardy, Italy, and São Paulo state, Brazil," Physica D **413**, 132693 (2020).
[6]D. Fanelli and F. Piazza, "Analysis and forecast of COVID-19 spreading in China, Italy and France," Chaos, Solitons Fractals **134**, 109761 (2020).
[7]E. Postnikov, "Estimation of COVID-19 dynamics? 'on a back-of-envelope': Does the simplest SIR model provide quantitative parameters and predictions?," Chaos, Solitons Fractals **135**, 109841 (2020).
[8]I. Cooper, A. Mondal, and C. Antonopoulos, "A SIR model assumption for the spread of COVID-19 in different communities," Chaos, Solitons Fractals **139**, 110057 (2020).
[9]W. Kermack and A. McKendrick, "A contribution to the mathematical theory of epidemics," Proc. R. Soc. London, Ser. A **115**, 700 (1927).
[10]E. Cuevas, "An agent-based model to evaluate the COVID-19 transmission risks in facilities," Comput. Biol. Med. **121**, 103827 (2020).
[11]P. C. Silva, P. V. Batista, H. S. Lima, M. A. Alves, F. G. Guimarães, and R. C. Silva, "COVID-ABS: An agent-based model of COVID-19 epidemic to simulate health and economic effects of social distancing interventions," Chaos, Solitons Fractals **139**, 110088 (2020).
[12]R. J. Rockett, A. Arnott, C. Lam, R. Sadsad, V. Timms, K.-A. Gray, J.-S. Eden, S. Chang, M. Gall, J. Draper, E. M. Sim, N. L. Bachmann, I. Carter, K. Basile, R. Byun, M. V. O'Sullivan, S. C.-A. Chen, S. Maddocks, T. C. Sorrell, D. E. Dwyer, E. C. Holmes, J. Kok, M. Prokopenko, and V. Sintchenko, "Revealing COVID-19 transmission in Australia by SARS-CoV-2 genome sequencing and agent-based modeling," Nat. Med. **26**, 1398 (2020).
[13]E. Hunter, B. M. Namee, and J. D. Kelleher, "A taxonomy for agent-based models in human infectious disease epidemiology," J. Artif. Soc. Soc. Simul. **20**(3), 2 (2017).
[14]S. He, Y. Peng, and K. Sun, "SEIR modeling of the COVID-19 and its dynamics," Nonlinear Dyn. **101**, 1667–1680 (2020).
[15]A. Ramos, M. Ferrández, M. Vela-Pérez, A. Kubik, and B. Ivorra, "A simple but complex enough theta-SIR type model to be used with COVID-19 real data. Application to the case of Italy," Physica D **421**, 132839 (2021).
[16]G. Giordano, F. Blanchini, R. Bruno, P. Colaneri, A. Di Filippo, A. Di Matteo, and M. Colaneri, "Modelling the COVID-19 epidemic and implementation of population-wide interventions in Italy," Nat. Med. **26**, 855–860 (2020).
[17]A. J. Kucharski, T. W. Russell, C. Diamond, Y. Liu, J. Edmunds, S. Funk, R. M. Eggo, F. Sun, M. Jit, J. D. Munday, N. Davies, A. Gimma, K. van Zandvoort, H. Gibbs, J. Hellewell, C. I. Jarvis, S. Clifford, B. J. Quilty, N. I. Bosse, S. Abbott, P. Klepac, and S. Flasche, "Early dynamics of transmission and control of COVID-19: A mathematical modelling study," Lancet Infect. Dis. **20**(5), 553 (2020).
[18]Q. Lin, S. Zhao, D. Gao, Y. Lou, S. Yang, S. S. Musa, M. H. Wang, Y. Cai, W. Wang, L. Yang, and D. He, "A conceptual model for the coronavirus disease 2019 (COVID-19) outbreak in Wuhan, China with individual reaction and governmental action," Int. J. Infect. Dis. **93**, 211 (2020).
[19]J. Grauer, H. Löwen, and B. Liebchen, "Strategic spatiotemporal vaccine distribution increases the survival rate in an infectious disease like COVID-19," Sci. Rep. **10**(1), 21594 (2020).
[20]A. Kouidere, D. Kada, O. Balatif, M. Rachik, and M. Naim, "Optimal control approach of a mathematical modeling with multiple delays of the negative impact of delays in applying preventive precautions against the spread of the COVID-19 pandemic with a case study of Brazil and cost-effectiveness," Chaos, Solitons Fractals **142**, 110438 (2021).
[21]Z. Liu, P. Magal, O. Seydi, and G. Webb, "A COVID-19 epidemic model with latency period," Infect. Dis. Modell. **5**, 323–337 (2020).
[22]M. Mahrouf, A. Boukhouima, H. Zine, E. Lotfi, D. Torres, and N. Yousfi, "Modeling and forecasting of COVID-19 spreading by delayed stochastic differential equations," Axioms **10**(1), 18 (2021).
[23]S. Vinitsky, A. Gusev, V. Derbov, P. Krassovitskiy, F. Penkov, and G. Chuluunbaatar, "Reduced SIR model of COVID-19 pandemic," Comput. Math. Math. Phys. **61**(3), 376–387 (2021).
[24]M. Naveed, M. Rafiq, A. Raza, N. Ahmed, I. Khan, K. Nisar, and A. Soori, "Mathematical analysis of novel coronavirus (2019-nCov) delay pandemic model," Comput., Mater. Continua **64**(3), 1401–1414 (2020).
[25]A. Kergaßner, C. Burkhardt, D. Lippold, M. Kergaßner, L. Pflug, D. Budday, P. Steinmann, and S. Budday, "Memory-based meso-scale modeling of COVID-19," Comput. Mech. **66**(5), 1069 (2020).
[26]F. Köhler-Rieper, C. H. F. Röhl, and E. De Micheli, "A novel deterministic forecast model for the COVID-19 epidemic based on a single ordinary integro-differential equation," Eur. Phys. J. Plus **135**(7), 599 (2020).
[27]G. Dimarco, B. Perthame, G. Toscani, and M. Zanella, "Kinetic models for epidemic dynamics with social heterogeneity," J. Math. Biol. **83**, 4 (2021).
[28]L. Guan, C. Prieur, L. Zhang, C. Prieur, D. Georges, and P. Bellemain, "Transport effect of COVID-19 pandemic in France," Annu. Rev. Control **50**, 394 (2020).
[29]X. Geng, G. G. Katul, F. Gerges, E. Bou-Zeid, H. Nassif, and M. C. Boufadel, "A kernel-modulated SIR model for COVID-19 contagious spread from county to continent," Proc. Natl. Acad. Sci. **118**(21), e2023321118 (2021).
[30]C. Cercignani, *Ludwig Boltzmann: The Man Who Trusted Atoms* (Oxford University Press, 1998).
[31]M. Falcioni and A. Vulpiani, "Ludwig Boltzmann: A tribute on his 170th birthday," Lett. Mat. **2**, 171 (2015).
[32]M. Ianniello and G. Israel, "Boltzmann's 'Nachwirkung' and hereditary mechanics," in *Proceedings of the International Symposium on Ludwig Boltzmann, Rome, February 9–11, 1989*, edited by G. Battimelli, M. Ianniello, and O. Kresten (Verlag der Österreichischen Akademie der Wissenschaften, 1993).
[33]R. Kohlrausch, "Ueber das Dellmann'sche Elektrometer (About the Dellmann electrometer)," Ann. Phys. **148**(11), 353 (1847) (in German).
[34]R. Kohlrausch, "Theorie des elektrischen Rückstandes in der Leidener Flasche (Theory of the electrical residue in the Leyden jar)," Ann. Phys. **167**(1), 56 (1854) (in German).
[35]R. Kohlrausch, "Theorie des elektrischen Rückstandes in der Leidener Flasche (Theory of the electrical residue in the Leyden jar)," Ann. Phys. **167**(2), 179 (1854) (in German).
[36]F. Kohlrausch, "Über die elastische Nachwirkung bei der torsion (About the elastic aftereffect of torsion)," Ann. Phys. **195**(7), 337 (1863).
[37]F. Kohlrausch, "Beiträge zur Kenntniss der elastischen Nachwirkung (Contributions to the knowledge of the elastic aftereffect)," Ann. Phys. **204**(5), 1 (1866) (in German).
[38]F. Kohlrausch, "Beiträge zur Kenntniss der elastischen Nachwirkung. Allgemeines über den untersuchten Silberdraht (Contributions to the knowledge of the elastic aftereffect. General information about the examined silver wire)," Ann. Phys. **204**(6), 207 (1866) (in German).
[39]F. Kohlrausch, "Beiträge zur Kenntniss der elastischen Nachwirkung. Abhängigkeit der Nachwirkung von der Größe und Dauer der vorangegangenen Verschiebung (Contributions to the knowledge of the elastic aftereffect. Dependency of the aftereffect on the size and duration of the previous shift)," Ann. Phys. **204**(7), 399 (1866) (in German).
[40]F. Kohlrausch, "Experimental-Untersuchungen über die elastische Nachwirkung bei der Torsion, Ausdehnung und Biegung (Experimental investigations on the elastic aftereffect of torsion, expansion and bending)," Ann. Phys. **234**(7), 337 (1876) (in German).
[41]W. Weber, "Ueber die Elasticität der Seidenfäden (About the elasticity of silk thread)," Ann. Phys. **110**(2), 247 (1835) (in German).
[42]W. Weber, "Ueber die Elasticität fester Körper (About the elasticity of solids)," Ann. Phys. **130**(9), 1–19 (1841) (in German).
[43]M. Gurtin and E. Sternberg, "On the linear theory of viscoelasticity," Arch. Ration. Mech. Anal. **11**, 291 (1962).
[44]J. Salençon, *Viscoélasticité (Viscoelasticity)* (Presses de l'Ecole Nationale des Ponts et Chaussées, 1983) (in French).
[45]R. Lakes, *Viscoelastic Solids* (CRC Press, 1999).
[46]J. Salençon, *Handbook of Continuum Mechanics* (Springer-Verlag Berlin Heidelberg, 2001).
[47]S. Scheiner and C. Hellmich, "Continuum microviscoelasticity model for aging basic creep of early-age concrete," J. Eng. Mech. **135**(4), 307 (2009).
[48]M. Irfan-ul Hassan, B. Pichler, R. Reihsner, and C. Hellmich, "Elastic and creep properties of young cement paste, as determined from hourly repeated minute-long quasi-static tests," Cem. Concr. Res. **82**, 36 (2016).
[49]J. Kolařík and A. Pegoretti, "Proposal of the Boltzmann-like superposition principle for nonlinear tensile creep of thermoplastics," Polym. Testing **27**(5), 596 (2008).
[50]L. Eberhardsteiner, C. Hellmich, and S. Scheiner, "Layered water in crystal interfaces as source for bone viscoelasticity: Arguments from a multiscale approach," Comput. Methods Biomech. Biomed. Eng. **17**(1), 48 (2014).

[51]S. Park and G. Ateshian, "Dynamic response of immature bovine articular cartilage in tension and compression, and nonlinear viscoelastic modeling of the tensile response," J. Biomech. Eng.-Trans. ASME **128**, 623–630 (2006).
[52]P. Verhulst, "Notice sur la loi que la population suit dans son accroissement (Notice on the law that the population growth follows)," Corresp. Math. Phys. **10**, 113 (1838) (in French).
[53]A. Tsoularis and J. Wallace, "Analysis of logistic growth models," Math. Biosci. **179**(1), 21 (2002).
[54]S. Strogatz, *Nonlinear Dynamics and Chaos: With Applications to Physics, Biology, Chemistry and Engineering*, 2nd ed. (CRC Press, 2015).
[55]S. Scheiner, N. Ukaj, and C. Hellmich, "Mathematical modeling of COVID-19 fatality trends: Death kinetics law versus infection-to-death delay rule," Chaos, Solitons Fractals **136**, 109891 (2020).
[56]A. Osemwynjen and A. Diakhaby, "Mathematical modeling of the transmission dynamics of Ebola virus," Appl. Comput. Math. **4**, 313 (2015).
[57]See www.corona-ks.info for "Coronavirus (SARS-CoV-2) Outbreak in Kosovo" (last accessed October 23, 2021).
[58]See www.worldometers.info/coronavirus for "COVID-19 Pandemic" (last accessed October 23, 2021).
[59]R. H. Byrd, M. E. Hribar, and J. Nocedal, "An interior point algorithm for large-scale nonlinear programming," SIAM J. Optim. **9**(4), 877 (1999).
[60]R. H. Byrd, J. C. Gilbert, and J. Nocedal, "A trust region method based on interior point techniques for nonlinear programming," Math. Program. **89**(1), 149 (2000).
[61]R. Waltz, J. Morales, J. Nocedal, and D. Orban, "An interior algorithm for nonlinear optimization that combines line search and trust region steps," Math. Program. **107**(3), 391 (2006).
[62]See https://de.mathworks.com/help/optim/index.html for "Matlab Optimization Toolbox, Version 9.0 R2020b" (last accessed October 23, 2021).
[63]L. Boltzmann, "Zur Theorie der elastischen Nachwirkung (Concerning the theory of the elastic aftereffect)," Sitzungsber. Math.-Naturwiss. Cl. Kais. Akad. Wiss. **70**(2), 275 (1874) (in German).
[64]H. Markovitz, "Boltzmann and the beginnings of linear viscoelasticity," Trans. Soc. Rheol. **21**(3), 381 (1977).
[65]J. Liu, L. Wang, Q. Zhang, and S.-T. Yau, "The dynamical model for COVID-19 with asymptotic analysis and numerical implementations," Appl. Math. Modell. **89**, 1965 (2021).
[66]N. Shao, M. Zhong, Y. Yan, H. Pan, J. Cheng, and W. Chen, "Dynamic models for coronavirus disease 2019 and data analysis," Math. Methods Appl. Sci. **43**(7), 4943 (2020).
[67]Y. Bai, L. Yao, T. Wei, F. Tian, D. Jin, L. Chen, and M. Wang, "Presumed asymptomatic carrier transmission of COVID-19," JAMA **323**(14), 1406 (2020).
[68]A. Singanayagam, M. Patel, A. Charlett, J. Lopez Bernal, V. Saliba, J. Ellis, S. Ladhani, M. Zambon, and R. Gopal, "Duration of infectiousness and correlation with RT-PCR cycle threshold values in cases of COVID-19, England, January to May 2020," Eurosurveillance **25**(32), 2001483 (2020).
[69]M. Massinga Loembé, A. Tshangela, S. Salyer, J. Varma, A. Ouma, and J. Nkengasong, "COVID-19 in Africa: The spread and response," Nat. Med. **26**(7), 999 (2020).
[70]V. Deshwal, "COVID 19: A comparative study of Asian, European, American continent," Int. J. Sci. Res. Eng. Dev. **3**, 436 (2020).
[71]M. Bubar, K. Reinholt, S. Kissler, M. Lipsitch, S. Cobey, Y. Grad, and D. Larremore, "Model-informed COVID-19 vaccine prioritization strategies by age and serostatus," Science **371**(6532), 916 (2021).
[72]A. Brufsky, "Distinct viral clades of SARS-CoV-2: Implications for modeling of viral spread," J. Med. Virol. **92**(9), 1386–1390 (2020).
[73]S. J. Kang and S. I. Jung, "Age-related morbidity and mortality among patients with COVID-19," Korean Soc. Infect. Dis. Korean Soc. Chemother. **52**(2), 154 (2020).
[74]P. Zimmermann and N. Curtis, "Why is COVID-19 less severe in children? A review of the proposed mechanisms underlying the age-related difference in severity of SARS-CoV-2 infections," Arch. Dis. Child. **106**(5), 429 (2021).
[75]V. Bajaj, N. Gadi, A. Spihlman, S. Wu, C. Choi, and V. Moulton, "Aging, immunity, and COVID-19: How age influences the host immune response to coronavirus infections?," Front. Physiol. **11**, 571416 (2021).
[76]M. Akbar, A. Wibowo, R. Pranata, and B. Setiabudiawan, "Low serum 25-hydroxyvitamin D (vitamin D) level is associated with susceptibility to COVID-19, severity, and mortality: A systematic review and meta-analysis," Front. Nutr. **8**, 660420 (2021).
[77]C. Gotluru, A. Roach, S. Cherry, and C. Runowicz, "Sex, hormones, immune functions, and susceptibility to coronavirus disease 2019 (COVID-19)-related morbidity," Obstet. Gynecol. **137**(3), 423 (2021).
[78]See https://www.ecdc.europa.eu/en/publications-data/data-covid-19-vaccination-eu-eea for "Data on COVID-19 Vaccination in the EU/EEA" (last accessed October 23, 2021).
[79]G. Kaniadakis, M. Baldi, T. Deisboeck, G. Grisolia, D. Hristopulos, A. Scarfone, A. Sparavigna, T. Wada, and U. Lucia, "The κ-statistics approach to epidemiology," Sci. Rep. **10**, 19949 (2020).
[80]G. Kaniadakis, "New power-law tailed distributions emerging in κ-statistics," Europhys. Lett. **133**, 10002 (2021).